Journal of Marine Research, 74, 277–313, 2016

Methane dynamics in Santa Barbara Basin (USA) sediments as examined with a reaction-transport model

by David J. Burdige,[1,2] Tomoko Komada,[3] Cédric Magen,[4] and Jeffrey P. Chanton[5]

ABSTRACT

Here we describe a new reaction-transport model that quantitatively examines $\delta^{13}C$ profiles of pore-water methane and dissolved inorganic carbon (DIC) ($\delta^{13}C_{CH4}$ and $\delta^{13}C_{DIC}$) in the anoxic sediments of the Santa Barbara Basin (California Borderland region). Best-fit solutions of the model to these data suggest that CO_2 reduction is the predominant form of methanogenesis in these sediments. These solutions also accurately reproduce the isotope depth profiles, including a broad minimum in the $\delta^{13}C_{DIC}$ profile and a much sharper (angular) minimum in the $\delta^{13}C_{CH4}$ profile, both of which appear near the base of the transition zone in the sediments between sulfate reduction and methanogenesis (referred to here as the sulfate-methane transition zone, or SMTZ). Such minima in pore-water profiles of $\delta^{13}C_{CH4}$ near the base of the SMTZ have been seen in a number of other marine sediments across a range of depth and timescales. We show here that this minimum in the $\delta^{13}C_{CH4}$ profile in Santa Barbara Basin sediments results from the balance between (1) anaerobic oxidation of methane (AOM), which leads to an increase in $\delta^{13}C_{CH4}$ with decreasing depth in the sediment column through and above the SMTZ; (2) methanogenesis, which produces ^{13}C-depleted methane, both in and below the SMTZ; and (3) an upward flux of CH_4 from depth that is relatively enriched in ^{13}C as compared with the methane in these pore waters. Possible sources of this deep methane include the following: geologic hydrocarbon reservoirs derived from ancient source rocks; decomposition of buried gas hydrates; and biogenic (or perhaps thermogenic) methane produced hundreds of meters below the seafloor stimulated by increasing temperatures associated with the sediment geothermal gradient. Although we are unable to resolve these possible sources of deep methane, we believe that the significance of an upward methane flux as an explanation for minima in $\delta^{13}C_{CH4}$ pore-water profiles may not be limited to Santa Barbara Basin sediments but may be common in many continental margin sediments.

Keywords: methane, anoxic sediments, stable isotopes, anaerobic oxidation of methane, reaction-transport model

1. Department of Ocean, Earth and Atmospheric Sciences, Old Dominion University, Norfolk, VA 23529.
2. Corresponding author: ***e-mail: dburdige@odu.edu***
3. Romberg Tiburon Center, San Francisco State University, 3150 Paradise Drive, Tiburon, CA 94920.
4. Chesapeake Biological Laboratory, University of Maryland Center for Environmental Science, 146 Williams Street, P.O. Box 38, Solomons, MD 20688.
5. Department of Earth, Ocean and Atmospheric Science, Florida State University, P.O. Box 3064520, Tallahassee, FL 32306-4520.

1. Introduction

The processes affecting methane cycling in marine sediments are important across a wide range of spatial and temporal scales. Methane (CH_4) is a greenhouse gas with a global warming potential of ~45 times that of CO_2 on a 100-year timescale (Neubauer and Megonigal 2015). The atmospheric CH_4 concentration (albeit at trace levels) has increased since the start of the Industrial Revolution, and it has therefore played a role in recent increases in global temperature (Houghton 2015). Although large amounts of methane are produced and stored in marine sediments today, almost 100% of the methane that diffuses upward toward the sediment surface is consumed, largely by anaerobic oxidation of methane (AOM), and results in little to no net methane export to the water column (Reeburgh 2007). However, this may not have always been true in the geologic past (Berner 2004; Payne et al. 2004; Dickens 2011; Gu et al. 2011), nor will it necessarily be true in the future in response to continued global warming (e.g., Archer 2007).

Modeling of methane cycling in sediments has tended to focus on examining methane oxidation, specifically AOM (Alperin, Reeburgh, and Whiticar 1988; Martens, Albert, and Alperin 1999; Hoehler et al. 2000; Ussler and Paull 2008; Lloyd, Alperin, and Teske 2011). In contrast, less work has been done directly modeling methane production (methanogenesis) (Blair, Boehme, and Carter 1993; Wallmann et al. 2006; Burdige 2011; Burdige et al. 2016a). Here we describe a stable isotope reaction-transport model (the SIRT model) that allows us to quantitatively examine pore-water $\delta^{13}C$ profiles of methane and dissolved inorganic carbon (DIC) ($\delta^{13}C_{CH4}$ and $\delta^{13}C_{DIC}$). This model builds on our previous modeling effort examining concentration profiles of DIC, methane, sulfate, and ammonium in anoxic sediments (the OMSN model; Burdige et al. 2016a). We applied this isotope model to data recently collected in the anoxic sediments of the Santa Barbara Basin, in the California Borderland region (Burdige et al. 2016a; Komada et al. 2016), to gain insights into the controls on methanogenesis and methane oxidation in sediments.

2. Background

a. Methanogenesis

In a general sense, biogenic production of methane (methanogenesis) from particulate organic carbon (POC) can be written as

$$POC \rightarrow L_3CO_2 + L_2CH_4, \tag{1}$$

where L_2 and L_3 depend on ox, the oxidation state of the carbon in POC (e.g., Burdige and Komada 2011; note that all parameters and variables used here are defined in Table 1). For example, if $ox = 0$ (i.e., POC is CH_2O), L_2 and L_3 are both one-half. In our past and present work, we have assumed $ox = -0.7$ (Burdige and Komada 2015; Burdige et al. 2016a), based on a compilation of results from a wide range of studies of naturally occurring organic matter (Burdige 2007; although also see recent discussions in Arning, van Berk,

Table 1. List of variables and parameters.

Term	Description	Value	Units
$ACP(z)$	Depth distribution of the rate of authigenic calcium carbonate precipitation	(a)	mM y^{-1}
$AOMr$	Rate of anaerobic oxidation of methane (AOM; see equation A1b)		
$AOM13$	Rate of anaerobic oxidation of ^{13}C methane (see equation 26)		mM y^{-1}
$AOM12$	Rate of anaerobic oxidation of ^{12}C methane (see equation 25)		mM y^{-1}
D_x^s	Bulk sediment diffusion coefficient for species x corrected for tortuosity (θ^2; see equation A11), using the modified Weissberg equation (Boudreau 1997): $D_x^s = \frac{D_x^o}{\theta^2} = \frac{D_x^o}{1-2\ln\varphi}$		cm^2 y^{-1}
D_x^o	Seawater, free solution diffusion coefficient for species x	(b)	cm^2 y^{-1}
D	Concentration of DIC, where $D = D12 + D13$	(c)	mM
DMP	Rate of DIC production attributable to methanogenesis (see equation A4a)		mM y^{-1}
$DMP13_{Acf}$	Rate of DIC production attributable to methanogenesis in the Acf kinetic model for methanogenesis (see equations 23 and A6a)		mM y^{-1}
$DMP13_{C2r}$	Rate of DIC production attributable to methanogenesis in the $C2r$ kinetic model for methanogenesis (see equations 19 and A5a)		mM y^{-1}
$D1x$	Concentration of ^{1x}C-DIC ($DI^{1x}C$) [$x = 2$ or 3]	(c)	mM
$\Im$	A parameter that converts carbon concentrations in units of wt% C to mM and is given by $\Im = 10^4 \cdot (\rho_{ds}/12)\frac{1-\varphi}{\varphi}$	(d)	mM wt% C^{-1}
f_S	A function that inhibits the occurrence of methanogenesis when sulfate concentrations are above some threshold value (see equations 29 or 30)	(d)	
G_i	Concentration of metabolizable particulate organic carbon (POC) in fraction i (i = 1–3)	(e)	wt% C
K_a	AOM half-saturation constant (Dale et al. 2008)	1	mM
k_{aom}	First-order rate constant for AOM	(f)	y^{-1}
k_i	First-order rate constant for G_i degradation (i = 1–3)	(f)	y^{-1}
K_{in}	A parameter that controls the steepness of the transition of f_S (equation 29) from 0 to 1 that occurs around the sulfate concentration S^*	(f)	mM
K_m	Half-saturation constant for organoclastic sulfate reduction (oSR) (Burdige and Komada 2011)	0.5	mM
L_2	Ratio of sulfate reduced per mole of POC oxidized during oSR or moles of methane produced per mole of POC oxidized during methane production, given by $L_2 = (4 - ox)/8$	0.59	

(Continued)

Table 1. Continued.

Term	Description	Value	Units
L_3	Ratio of the moles of DIC produced per mole of POC consumed during methane production, given by $L_3 = (4 + ox)/8 = 1 - L_2$	0.41	
M	Concentration of methane, where $M = M12 + M13$	(c)	mM
MP	Rate of methane production (see equations 12 and A1a)		mM y^{-1}
$MP13_{Acf}$	Rate of ^{13}C-methane production in the *Acf* kinetic model for methanogenesis (see equations 22 and A3a)		mM y^{-1}
$MP13_{C2r}$	Rate of ^{13}C-methane production in the *C2r* kinetic model for methanogenesis (see equations 16 and A2a)		mM y^{-1}
$M1x$	Concentration of ^{1x}C methane ($^{1x}CH_4$) ($x = 2$ or 3)	(c)	mM
ox	Carbon oxidation state in POC	−0.7	
r^{13}_{Gi}	^{13}C/C ratio in POC fraction G_i; derived from δ_i as described in Komada et al. (2013)		
S	Concentration of sulfate	(c)	mM
$S*$	The sulfate concentration around which f_S transitions from 0 to 1 (see equation 29)	(f)	mM
z	Sediment depth (positive downward)		cm
α_{Acf}	Methanogenesis fractionation factor in the *Acf* kinetic model (see equation 21)	(g)	
α_{AOM}	AOM fractionation factor (see equation 25)	(g)	
α_{C2r}	Methanogenesis fractionation factor in the *C2r* kinetic model (see equation 15)	(g)	
δ_i	δ^{13}C value for G_i ($i = 1-3$)	(g)	‰
δ_{JlbD}	δ^{13}C value of the basal diffusive DIC flux	(g)	‰
δ_{JlbM}	δ^{13}C value of the basal diffusive methane flux	(g)	‰
ε_C	Isotope separation factor (see equation 2)		‰
ν	Porewater advection	(d)	cm y^{-1}
φ	Sediment porosity	(h)	
ω	Sediment accumulation (burial) rate	(d)	cm y^{-1}

Notes: (a) See the Appendix and Burdige et al. (2016a) for a discussion of this depth-dependent function. (b) See Table 2. (c) Dependent variable. (d) For these parameters, a single value is not used because the parameter changes either directly or indirectly with depth. In the latter case, for example, because porosity (φ) varies with sediment depth, so does $\Im$ and the various D_s values (because they are all a function of φ). For details, see Burdige et al. (2016). (e) Depth profiles of each G_i fraction were obtained by solving the reaction-transport equation for each fraction (equation A8) during the course of fitting the OMSN (organic matter/sulfate/nitrogen) model to the inorganic pore-water results (Burdige et al. 2016). (f) A best-fit parameter obtained by fitting the OMSN model to the inorganic pore-water results (Burdige et al. 2016). (g) Adjustable fitting parameter in the SIRT (stable isotope reaction-transport) model. (h) Porosity variations as a function of depth are reported in Komada et al. (2016). Also see equation (A13).

and Schulz 2016). Such a value of *ox* indicates that the organic material is H enriched and O depleted relative to cellulose/carbohydrate (CH_2O).

Methanogenesis typically occurs once sulfate is depleted, and in early diagenesis, reaction-transport (RT) models the rates of methane production and DIC production by methanogenesis are generally expressed as being first order with respect to the amount of reactive organic matter present, corrected for the stoichiometry of equation (1) (e.g., see equations 12 and 14). In actuality, though, methanogenesis (equation 1) is a multistep process (e.g., Fenchel, King, and Blackburn 1998; Megonigal, Hines, and Visscher 2003; Burdige and Komada 2015) in which POC is sequentially broken down first into smaller molecules by hydrolysis and/or oxidative cleavage followed by fermentation, eventually leading to CO_2, H_2, and a limited number of small organic molecules (e.g., acetate). When sulfate is absent, these compounds are then used in the terminal remineralization process by methanogenic bacteria to make methane. In most marine sediments, methanogenesis specifically occurs by CO_2 reduction (also sometimes referred to as carbonate reduction or hydrogenotrophic methanogenesis because H_2 is consumed in this process; see equation 6) and acetate fermentation (also sometimes referred to as acetate dissimilation or acetoclastic methanogenesis; see equation 20). Although there are other forms of methanogenesis, involving what are often referred to as noncompetitive substrates, for example methyl amines (see Kelley et al. 2014; Kelley, Chanton, and Bebout 2015; and references therein), CO_2 reduction and acetate fermentation are generally the predominant types of methanogenesis that occur in most anoxic aquatic environments (Whiticar 1999).

As a general rule, CO_2 reduction dominates methanogenesis in marine sediments, whereas acetate fermentation dominates in freshwater systems (Blair 1998; Whiticar 1999; Hornibrook, Longstaffe, and Fyfe 2000; Canfield, Thamdrup, Kristensen 2005; Conrad 2005). Substrate (organic carbon) availability and availability of more efficient oxidants (i.e., sulfate in marine systems) appear to play major roles here, with low substrate availability and/or high availability of these other oxidants tending to favor the occurrence of CO_2 reduction. Although these controlling factors generally tend to divide these two pathways of methanogenesis between marine and freshwater settings, there are a number of exceptions to this general trend (see any of the studies cited previously for details).

Methanogenesis strongly fractionates carbon isotopes such that the methane being produced is notably depleted in ^{13}C relative to the substrate and therefore has very negative $\delta^{13}C$ values, less than –60‰ (Whiticar 1999; Conrad 2005). The resulting DIC is therefore enriched in ^{13}C and has a much more positive $\delta^{13}C$ value than that of methane. In the environment, we can describe this fractionation in terms of the isotope separation factor (ε_C) between DIC and methane as follows:

$$\varepsilon_C = \delta^{13}C_{DIC} - \delta^{13}C_{CH4}, \tag{2}$$

where ε_C is typically less than 55‰ for acetate fermentation and greater than 65‰ for CO_2 reduction (Whiticar 1999). Thus, although CO_2 reduction tends to fractionate carbon

isotopes more than acetate fermentation, the controls on this fractionation, especially in the environment, are not fully understood.

b. Kinetic isotope fractionation

If a reaction with rate R fractionates the isotopes of reactant C, then we can define a fractionation factor α as

$$\alpha = \frac{R_L/C_L}{R_H/C_H}, \tag{3}$$

(e.g., Rees 1973; Chernyavsky and Wortmann 2007) where the subscripts L and H represent the light (e.g., ^{12}C) and heavy (e.g., ^{13}C) isotopes, respectively. If, for example, this reaction is assumed to be a first-order process with respect to C, this equation can be simplified such that α represents the ratio of the two associated rate constants (i.e., $k_{L/}k_H$; Whiticar 1999). Based on this equation, R_H is given by,

$$R_H = \frac{C_H}{\alpha C - (\alpha - 1)C_H} R \tag{4}$$

where $R = R_H + R_L$ and $C = C_L + C_H$.

3. Field data

a. Study site and sample collection

The pore-water data examined here were obtained from sediment cores collected in the center of Santa Barbara Basin (590 m water depth), one of the inner basins of the California Borderland (Emery 1960). Santa Barbara Basin is low in dissolved O_2 below the basin sill depth of 475 m (Sholkovitz 1973), and these low bottom-water oxygen concentrations result in sediments in the central part of the basin being anoxic and varved (Soutar and Crill 1977; Reimers et al. 1996). The bottom-water dissolved O_2 concentration at the time of our sampling was $\sim$2 μmol kg^{-1} (Komada et al. 2016).

Sediment cores were collected using a gravity corer and a multicorer onboard R/V *Robert Gordon Sproul* in August 2012, and R/V *New Horizon* in August 2013. Details about coring and pore-water collection, processing, and analysis can be found in Komada et al. (2016). Because all these data have been described previously (Komada et al. 2016), only a very brief description of these results is presented in the next section.

b. Field results

Sulfate, methane, and DIC pore-water profiles indicate that sulfate reduction occurs in the upper $\sim$125 cm of Santa Barbara Basin sediments (referred to as the SO_4^{2-} zone), and that methanogenesis occurs below this depth (Fig. 1). From these observations, we defined the 125 $\pm$ 20 cm depth interval as the sulfate-methane transition zone (SMTZ) (Komada et al.

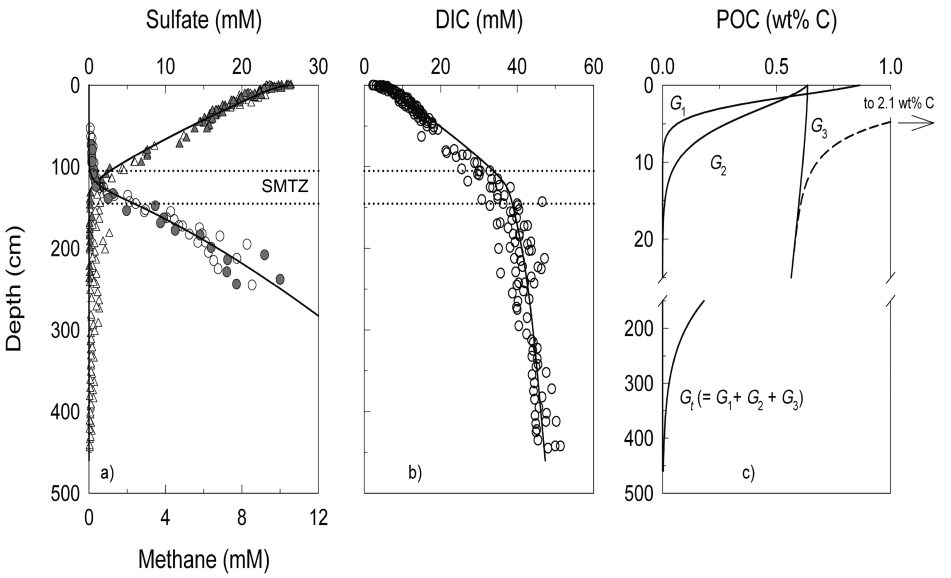

Figure 1. Depth profiles of pore-water sulfate and methane (a) and dissolved inorganic carbon (DIC) (b) concentrations in Santa Barbara Basin sediments (data from Komada et al. 2016). Closed symbols are 2012 data, open symbols are 2013 data, and samples from each year represent data from several cores (multicores and gravity cores). In panel (a), sulfate symbols are triangles, and methane symbols are circles. In all three panels, the solid lines represent the best fit of the OMSN (organic matter/sulfate/nitrogen) model to the data (Burdige et al. 2016a). The horizontal dotted lines here and in all other figures at 105 cm and 145 cm represent the upper and lower limits of the sulfate-methane transition zone (SMTZ) as defined in Komada et al. (2016). Concentrations of total reactive organic carbon (G_t) and reactive carbon in the G_1, G_2, and G_3 fractions (c); the latter are based on results from the fit of the OMSN model to the inorganic pore-water results (see equation A8 and discussions in Burdige et al. 2016a). POC, particulate organic carbon.

2016). Both the DIC and SO_4^{2-} profiles show curvature in the uppermost ~30 cm of sediment and in the SMTZ but were approximately linear in between. The DIC profile also showed a distinct slope break across the SMTZ, which is likely due to a combination of a decreased rate of DIC production (per mole of POC oxidized) in the deeper methanogenic sediments and an enhanced rate of DIC production in the SMTZ by AOM. Methane concentrations are <1 mM above the SMTZ but increase sharply through this zone. Curvature in the methane profile through the SMTZ is consistent with the occurrence here of AOM (Reeburgh 2007).

At the base of the pore-water DIC profile (4.6 m below the seafloor), the data indicate the occurrence of a small upward diffusive DIC flux, which was incorporated into a model of the DIC results as a flux boundary condition at the lower boundary (Burdige et al. 2016a). The methane data have also been modeled assuming there is an upward flux of methane from below the lower boundary. This is based on observations in Santa Barbara Basin sediments (Burdige et al. 2016a) and nearby Santa Monica Basin sediments (Burdige and Komada

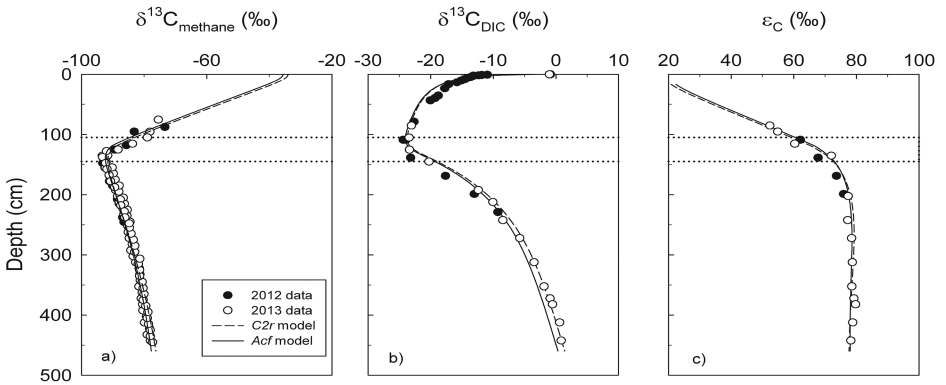

Figure 2. Depth profiles of pore-water $\delta^{13}C_{CH4}$ (a) and $\delta^{13}C_{DIC}$ (b) in Santa Barbara Basin sediments (data from Komada et al. 2016), along with best fits of the SIRT (stable isotope reaction-transport) model (using either the *C2r* or *Acf* kinetic expressions for methanogenesis) to the data. Best-fit parameters are listed in Table 3. (c) Depth profiles of the dissolved inorganic carbon (DIC)–methane isotope separation factor, ε_C, calculated using equation (2). Shown here are values derived from the model results in panels (a) and (b), along with calculated values based on pore-water data. There are fewer results here than in either panels (a) or (b) because we do not have matched pairs of isotope results for all samples.

2011), which show that the slopes of pore-water sulfate/DIC property-property plots cannot be explained without the existence of an external source of methane to the sediments that is uncoupled from contemporaneous surface organic carbon fluxes. Decomposing gas hydrates are one possibility for this source, although another possibility is biogenic (or perhaps thermogenic) methane production hundreds of meters below the seafloor stimulated by increasing sediment temperatures associated with the sediment geothermal gradient (see Sections 6a.ii and 6b for details).

Values of $\delta^{13}C_{DIC}$ decreased with sediment depth from approximately $-1‰$ in the bottom water to a broad minimum of $-24‰$ in the SMTZ and then increased with depth to $+1‰$ at the base of the profile (Fig. 2b). The decrease in $\delta^{13}C_{DIC}$ from the sediment surface to the SMTZ is consistent with production of isotopically light (^{13}C-depleted) DIC from (a) remineralization without isotope fractionation of marine POC, whose $\delta^{13}C$ value is typically approximately $-21‰$, by organoclastic sulfate reduction (oSR; see Section 4b), and (b) AOM, which fractionates against $^{13}CH_4$ and therefore produces extremely ^{13}C-depleted DIC from the ^{13}C-depleted CH_4 diffusing into the SMTZ (Fig. 2a). The increase in $\delta^{13}C_{DIC}$ below the SMTZ is consistent with the addition of isotopically heavy (^{13}C-enriched) DIC with depth, given the known carbon isotope fractionation associated with methanogenesis by either CO_2 reduction or acetate fermentation (Whiticar 1999; Conrad 2005).

Above the SMTZ, $\delta^{13}C_{CH4}$ increased with decreasing depth from a sharp minimum of approximately $-94‰$ (Fig. 2). This enrichment of $^{13}CH_4$ above the SMTZ, which occurs as

methane is consumed by AOM, is consistent with the known isotope fractionation associated with AOM (see Section 4b; Alperin, Reeburgh, and Whiticar 1988; Whiticar 1999; Conrad 2005). The increase in $\delta^{13}C_{CH4}$ with depth below the SMTZ is consistent with the occurrence of methanogenesis via CO_2 reduction when the substrate DIC also becomes increasingly enriched in ^{13}C with depth (Whiticar 1999, and references therein). This increase in $\delta^{13}C_{CH4}$ may also be related to the occurrence of an upward flux of CH_4 from depth (i.e., below the lower model boundary) that is relatively enriched in ^{13}C as compared with the CH_4 in these pore waters. This point will be discussed in greater detail in Sections 6a.ii and 6b.

4. Model formulation

The SIRT model described here is a steady-state RT model based on a similar model (the OMSN model) for pore-water sulfate (S), DIC (D), methane (M), ammonium (A), and calcium (Ca) and reactive solid phase POC (POC or G in the model equations). The OMSN model is described in detail in Burdige et al. (2016a). Both models assume that there are three pools of reactive organic matter undergoing remineralization, and model equations include the following: the transport processes diffusion, sediment burial, and pore-water advection driven by sedimentation and compaction; POC remineralization by oSR and methanogenesis; AOM; ammonium regeneration coupled to oSR and methanogenesis; and authigenic calcium carbonate precipitation. Rate expressions for these biogeochemical processes are discussed in the Appendix and in Burdige et al. (2016a).

Equations for $D13$ ($DI^{13}C$) and $M13$ ($^{13}CH_4$) in the SIRT model were based on the analogous equations for total DIC and methane in the OMSN model, with rate expressions modified as described subsequently to take into account methane and DIC carbon isotope fractionation associated with methanogenesis and AOM, $DI^{13}C$ production during oSR, and $DI^{13}C$ removal by authigenic carbonate precipitation. The equations in the SIRT model are listed in the Appendix.

a. Kinetic models for methane formation and isotope fractionation

In this section, we develop kinetic models for methane production and the associated carbon isotopic fractionation during the two primary types of methanogenesis. We call these the "CO_2 reduction" model ($C2r$) and the "acetate fermentation" model (Acf).

i. CO_2 reduction model (C2r) Here we assume that methanogenesis can be written as a two-step process (e.g., Shoemaker and Schrag 2010; Archer, Buffett, and McGuire 2012):

$$POC \rightarrow CO_2 + \frac{4 - ox}{2} H_2 \tag{5}$$

$$CO_2 + 4H_2 \rightarrow CH_4 + 2H_2O. \tag{6}$$

Because the oxidation state of the carbon in POC is taken to be ox (see Section 2a and Table 1), if, for example, $ox = 0$, then 2 moles of H_2 are produced per mole of POC

oxidized. With $ox = -0.7$, equation (5) makes slightly more hydrogen per mole of POC oxidized.

The rate of *POC* consumption in equation (5) is written as follows (e.g., Berner 1980; Burdige et al. 2016a):

$$\frac{dG}{dt} = -kG, \tag{7}$$

while DIC production in equation (5) is

$$\left.\frac{dD}{dt}\right|_{\text{prod}} = kG, \tag{8}$$

and H_2 production is

$$\left.\frac{d\text{H}_2}{dt}\right|_{\text{prod}} = \frac{4 - ox}{2} kG = 4L_2kG. \tag{9}$$

We next assume that there is a very tight coupling between H_2 production and consumption in this reaction sequence. This results in pore-water H_2 concentrations being kept at very low levels, which is a common observation in anoxic marine sediments (Lovley and Goodwin 1988; Hoehler et al. 1998) and further allows us to assume that H_2 production and consumption at any sediment depth are always equal one another. If we define R_{HC} as the rate of H_2 consumption in equation (6), then the net production of H_2 is

$$\left.\frac{d\text{H}_2}{dt}\right|_{\text{net}} \equiv 0 = 4L_2kG - R_{\text{HC}}, \tag{10}$$

and therefore,

$$R_{\text{HC}} = 4L_2kG. \tag{11}$$

Based on the stoichiometry of equation (6), the rate of methane production (*MP*) is then

$$\frac{dM}{dt} = {}^1\!/_4 R_{\text{HC}} = L_2kG (\equiv MP) \tag{12}$$

Note that this kinetic expression is identical to the rate expression for methanogenesis used in the OMSN model (Burdige et al. 2016a; also see equation A1a in the Appendix).

Mass balance in equation (6) indicates that DIC consumption is given by

$$\left.\frac{dD}{dt}\right|_{\text{cons}} = \frac{dM}{dt} = L_2kG, \tag{13}$$

and that net DIC production by the two-step $C2r$ process (combining equations 8 and 13) is

$$\left.\frac{dD}{dt}\right|_{\text{net}} = kG - L_2kG = (1 - L_2)kG = L_3kG \tag{14}$$

because $1 - L_2 = L_3$ (Table 1). Again this equation is identical to the expression for DIC production (from methanogenesis) used in the RT equations in the OMSN model (Burdige et al. 2016a; also see equation A4a in the Appendix).

To derive the corresponding expressions for $^{13}CH_4$ ($M13$) and net $DI^{13}C$ ($D13$) production by equations (5) and (6), we assume that there is no isotope fractionation during equation (5) (e.g., Corbett et al. 2013a) and that all fractionation occurs solely during equation (6). Based on equation (3), the α value for equation (6) is

$$\alpha_{\text{C2r}} = \frac{MP12/D12}{MP13/D13}, \tag{15}$$

where $MP1x$ is the rate of methane ($^{1x}CH_4$) production from $DI^{1x}C$, and $D1x$ is the concentration of $DI^{1x}C$.

Based on equation (3), $MP13$ in the $C2r$ process is given by

$$MP13_{\text{C2r}} = \frac{D13}{\alpha_{\text{C2r}}D - (\alpha_{\text{C2r}} - 1)D13}MP = \left(\frac{D13}{\alpha_{\text{C2r}}D - (\alpha_{\text{C2r}} - 1)D13}\right)L_2kG, \tag{16}$$

where D equals $D12 + D13$.

For net production of $D13$ by the $C2r$ process, we first remember that there is no fractionation during equation (5) (i.e., the initial production of $D13$). Therefore, the initial production of $D13$ will be proportional to the concentration of $PO^{13}C$ (^{13}G) as in equation (6):

$$\left.\frac{dD13}{dt}\right|_{\text{prod}} = kr_G^{13}G, \tag{17}$$

where $^{13}G = r_G^{13}G$ and

$$r_G^{13} = (^{13}C/C)_G. \tag{18}$$

This ratio is ultimately determined from the $\delta^{13}C$ value of the organic matter (G) producing methane (for details, see, e.g., Komada et al. 2013). By analogy with equation (13), $\frac{dM13}{dt} = \left.\frac{dD13}{dt}\right|_{\text{cons}}$, and recalling that $\frac{dM13}{dt}$ is the same as $MP13$, net $D13$ production by the $C2r$ process ($DMP13_{\text{C2r}}$) is the difference between equations (17) and (16):

$$DMP13_{\text{C2r}} = k\, r_G^{13}\, G - \left(\frac{D13}{\alpha_{\text{C2r}}D - (\alpha_{\text{C2r}} - 1)D13}\right)L_2\, kG. \tag{19}$$

ii. Acetate fermentation model (Acf) In the *Acf* model, we assume that methanogenesis is approximated by

$$POC \rightarrow \text{acetate} \rightarrow L_3CO_2 + L_2CH_4, \tag{20}$$

where L_2 and L_3 are defined in Table 1 (also see equation 1). Here we assume that there is no overall fractionation during acetate production from *POC* (Conrad 2005; Heuer et al. 2010; Conrad et al. 2014), although there may be intramolecular fractionation between the methyl and carboxyl groups during acetate production (Blair, Martens, and DesMarais 1987; Alperin et al. 1992). Any such fractionation, plus any fractionation associated with subsequent methane production by the second half of equation (20), is included in an α value for the entire process. Ultimately, this implies that in the *Acf* model there is instantaneous isotope mass balance between the original *POC* and the methane and DIC products (see related discussion in Blair 1998; Corbett et al. 2013b).

Based on equation (3), the α value for methane production in the *Acf* model is

$$\alpha_{\text{Acf}} = \frac{MP12/{}^{12}G}{MP13/{}^{13}G}. \tag{21}$$

A comparison of this equation with equation (15) illustrates the key difference between the *C2r* and *Acf* models—namely, that fractionation in the latter model is expressed relative to the parent organic matter, whereas in the former it is expressed relative to the DIC pool. The significance of this will be discussed further in the beginning of Section 6.

With this definition of α_{Acf}, equations (4) and (12) can be used to express $MP13$ during acetate fermentation as

$$\begin{aligned} MP13_{\text{Acf}} &= \frac{{}^{13}G}{\alpha_{\text{Acf}}G - (\alpha_{\text{Acf}} - 1){}^{13}G} MP = \left(\frac{r_G^{13}}{\alpha_{\text{Acf}} - (\alpha_{\text{Acf}} - 1) r_G^{13}} \right) MP \\ &= \left(\frac{r_G^{13}}{\alpha_{\text{Acf}} - (\alpha_{\text{Acf}} - 1) r_G^{13}} \right) L_2 kG. \end{aligned} \tag{22}$$

The production of $D13$ via acetate fermentation is then equal to the total loss of ${}^{13}G$ minus that which is converted to $M13$ (i.e., equation 22), and so,

$$DMP13_{\text{Acf}} = k\, r_G^{13} G - \left(\frac{r_G^{13}}{\alpha_{\text{Acf}} - (\alpha_{\text{Acf}} - 1) r_G^{13}} \right) L_2 kG \tag{23}$$

b. Isotope fractionation during AOM, oSR, and authigenic carbonate precipitation

AOM can be written as

$$CH_4 + SO_4^{2-} \rightarrow HCO_3^- + HS^- + H_2O \tag{24}$$

and is known to fractionate against $^{13}CH_4$ producing DIC that is depleted in ^{13}C and leaving behind methane that is enriched in ^{13}C (Alperin et al. 1988; Whiticar 1999). Therefore, AOM isotope fractionation must also be incorporated into the RT equations for $D13$ and $M13$.

Based on equation (3),

$$\alpha_{AOM} = \frac{AOM12/M12}{AOM13/M13} \tag{25}$$

and based on equation (4), $AOM13$ (the rate of anaerobic oxidation of $^{13}CH_4$) is given by

$$AOM13 = \frac{M13}{\alpha_{AOM}M - (\alpha_{AOM} - 1)M13}AOMr, \tag{26}$$

where $AOMr$ is the rate of total AOM ($= AOM12 + AOM13$; see equation A1b in the Appendix).

In contrast, we assume that there is no carbon isotope fractionation during oSR (Boehme et al. 1996; Lapham, Proctor, and Chanton 1999; Corbett et al. 2013a):

$$POC + L_2SO_4^{2-} \rightarrow HCO_3^- + L_2HS^-, \tag{27}$$

where L_2 also represents the moles of sulfate reduced per mole of POC oxidized (see Table 1). The production of $D13$ by oSR is therefore obtained by multiplying the rate expression for total oSR by the value of r_G^{13} (equation 18) for the organic matter being degraded (e.g., compare the relevant rate expression for oSR in equation A4 with that in either equation A5 or A6).

Finally, our previous results (Komada et al. 2016) and those of earlier studies of Santa Barbara Basin sediments (Sholkovitz 1973; Reimers et al. 1996; Berelson et al. 2005) all show decreases in pore-water Ca^{2+} with sediment depth, which have been interpreted as being the result of authigenic calcium carbonate precipitation,

$$Ca^{2+} + CO_3^{2-} \rightarrow CaCO_3(s). \tag{28}$$

Because carbonate precipitation does not result in significant ^{13}C fractionation (Zeebe and Wolf-Gladrow 2001), we simply multiply the depth-dependent rate of carbonate precipitation, $ACP(z)$, by the ratio $D13/D$ to account for the loss of pore-water $DI^{13}C$ by carbonate precipitation (for details, see the next section and equations A5 and A6 in the Appendix).

c. RT model

The RT equations for $D13$ and $M13$ in the SIRT model were based on the analogous equations for total DIC and CH_4 in the OMSN model, with rate expressions for the relevant reactions modified as discussed previously to take into account isotope fractionation associated with these processes. Separate sets of RT equations in the SIRT model were used for the two different kinetic models of methanogenesis described in the previous sections. These RT equations are listed in the Appendix.

Table 2. Diffusion coefficients and bottom-water concentrations.

Solute	D^o (cm^2 y^{-1})[a]	C^o (mM)	δ^{13}C (‰)
DIC (HCO_3^-)	192.1	2.3[b]	−0.95[b]
Methane	275.2	0[c]	[d]

Notes: [a] Seawater, free solution diffusion coefficients at 5°C (bottom-water temperature). Taken from Schulz and Zabel (2006). Diffusion coefficients for dissolved inorganic carbon (DIC) and methane were used for DI^{13}C and $^{13}CH_4$. [b] Average bottom-water values measured in hydrocast samples (Komada et al. 2016). $D13$ in the bottom waters was determined with standard isotope equations using the bottom-water DIC C^o and δ^{13}C values listed here. [c] Assumed bottom-water value (see Sections 4d and 5). [d] Based on our assumed bottom-water methane concentration, this value is undefined (also see Section 5).

In the SIRT model equations, the kinetic rate expressions for $C2r$ and Acf derived in Sections 4a.i and 4a.ii are written as the sum of equations for each of the three fractions of organic matter undergoing remineralization (e.g., see equations such as A1a or A2a in the Appendix for details). Rate expressions in the Appendix convert rates of solid POC loss to rates of soluble DIC and methane production, using the parameter $\Im$ defined in Table 1. Rate equations for methanogenesis were also modified to account for the fact that methanogenesis is inhibited when sulfate concentrations are above some threshold concentration. This is done using the inhibition function f_S, which equals 0 above some threshold sulfate concentration and equals 1 below this threshold concentration (Table 1). This function is discussed in greater detail in Section 6a.i.

d. Fitting the model to the isotope data

To solve the SIRT model (i.e., equations A2 and A3 or A5 and A6), we used results from fits of the OMSN model (Burdige et al. 2016a) to the major solute data (sulfate, methane, and DIC) collected from the same cores from which the pore-water isotope data ($\delta^{13}C_{DIC}$ and $\delta^{13}C_{CH4}$) came (see Table A1 in the Appendix for a list of the best-fit parameters obtained by fitting the OMSN model to this major solute data). Note that the RT equations from the OMSN model for the three major solutes are also included in the Appendix. As with the OMSN model, the RT equations for $M13$ and $D13$ in the SIRT model were solved numerically in MATLAB using finite difference approximations and the method of lines technique with variable grid spacing (Schiesser 1991; Boudreau 1997; Burdige et al. 2016a). A complete copy of the MATLAB script of the model is available from the corresponding author.

The upper boundary condition of the model solutions was measured ($D13$) or assumed ($M13$) bottom-water concentrations (Table 2), while a diffusive flux boundary condition was applied at the base (4.6 m) of the model domain (see Sections 3b and the Appendix for details). These basal fluxes were based on the diffusive fluxes of total methane and DIC obtained with the OMSN model (see Table A1 in the Appendix), and the δ^{13}C values of the

basal fluxes, which were adjustable parameters used to fit the SIRT model to the isotope data.

Fitting the SIRT model to the pore-water isotope data involved first converting model-derived depth profiles of $D13$ and $M13$ to depth profiles of $\delta^{13}C_{DIC}$ and $\delta^{13}C_{CH4}$ using OMSN model results and standard equations for δ notation. Model-derived isotope depth profiles were then fit to the $\delta^{13}C_{DIC}$ and $\delta^{13}C_{CH4}$ pore-water data by adjusting the following: the $\delta^{13}C$ values of the three organic matter fractions undergoing remineralization (δ_i); the fractionation factors for methanogenesis (α_{C2r} or α_{Acf}, depending on which set of kinetic expressions were being used in the model equations); α_{AOM}; and the $\delta^{13}C$ values of the upward, basal methane and DIC fluxes (δ_{JlbM} and δ_{JlbD}, respectively). The best-fit values of these parameters were obtained using a Monte Carlo fitting technique described in Burdige et al. (2016a).

5. Model results

Best-fit solutions of the SIRT model to the Santa Barbara Basin sediment isotope data using either the $C2r$ or the Acf kinetic expressions for methanogenesis resulted in near-identical fits of the models that accurately reproduced the $\delta^{13}C_{CH4}$ and $\delta^{13}C_{DIC}$ profiles (Fig. 2). For $\delta^{13}C_{CH4}$, the r^2 values of the fits to the data were $\sim$0.91, while the r^2 values for the fits to the $\delta^{13}C_{DIC}$ data were $\sim$0.95. In and around the SMTZ, the model fits reproduced the broad subsurface minimum in the $\delta^{13}C_{DIC}$ depth profile and the much sharper (angular) minimum in the $\delta^{13}C_{CH4}$ depth profile.

As the isotope models are currently formulated they cannot estimate the value of $\delta^{13}C_{CH4}$ in the bottom waters because we assume that the methane concentration in the bottom waters is zero (Table 2), and therefore, $\delta^{13}C_{CH4}$ at $z = 0$ cm is undefined. However, the model-derived value of $\delta^{13}C_{CH4}$ just below the sediment-water interface is around $-40‰$ (Fig. 2), which agrees well with $\delta^{13}C$ values of the trace levels of methane in Santa Barbara Basin bottom water and surface sediment (5 cm) pore waters, which collectively range from –20‰ to –60‰ (Kessler et al. 2008). Furthermore, given the range of methane concentrations we see in the sediments (0 to up to $\sim$9–10 mM; see Fig. 1), the measured methane concentration in Santa Barbara Basin bottom water, $\sim$40–50 nM (Kessler et al. 2008), is indistinguishable from 0 mM within the context of our pore-water and model results.

Model results predict $\delta^{13}C$ values for the three fractions of organic matter undergoing remineralization in these sediments (i.e., δ_1–δ_3) that range from –20.7‰ to –21.3‰ (Table 3). These values agree well with similar estimates of these quantities based on modeling pore-water dissolved organic carbon (DOC) concentrations and isotope depth profiles from these sediments (–20.8‰ to –22.6‰; Burdige et al. 2016b), as well as with the $\delta^{13}C$ value of reactive POC in these sediments (–20.5 $\pm$ 0.6‰) determined with an isotope mixing-reaction plot (Komada et al. 2016). Similarly, an estimate of the $\delta^{13}C$ of the upward DIC flux based on an isotope mixing-reaction plot for pore-water DIC (45 $\pm$ 3‰; Komada et al. 2016) is close to, but smaller than, model-derived estimates here of the same quantity, δ_{JlbD} (70 $\pm$

Table 3. Summary of fitting results.

Parameter	*C2r* model	*Acf* model
δ_1	-21.1 ± 1.2‰	-21.3 ± 1.1‰
δ_2	-20.7 ± 1.5‰	-21.1 ± 1.1‰
δ_3	-20.8 ± 1.0‰	-20.9 ± 0.9‰
δ_{JIbD}	69.5 ± 9.7‰	69.6 ± 8.5‰
δ_{JIbM}	-68.0 ± 1.8‰	-64.3 ± 1.4‰
α_{C2r}	1.109 ± 0.003	
α_{Acf}		1.103 ± 0.003
α_{AOM}	1.008 ± 0.001	1.008 ± 0.001

Note: See model results in Figure 2.

10‰; see Table 3). However, a fit of the model to the data is not terribly sensitive to the isotopic composition of this DIC flux (also see Section 6a.ii), and using either value of δ_{JIbD} (i.e., 45‰ or 70‰) in model fits results in values of the remaining fitting parameters that agree with one another to within 1 standard deviation (results not shown here).

Model-derived values of α_{C2r} and α_{Acf} are very similar to each other (1.109 ± 0.003 and 1.103 ± 0.003, respectively; Table 3). Recall, however, that the former defines isotope fractionation associated with methanogenesis relative to fractionation of the DIC pool, whereas the latter defines this fractionation relative to the sediment POC pool (compare equations 15 and 21). Ignoring for now possible explanations for the similarities in the α_{C2r} and α_{Acf} values, despite the differences in the ways they are defined (which are discussed in the beginning of Section 6), these two α values fall within the range of values typically observed for methanogenesis via CO_2 reduction ($\alpha > 1.065$) versus acetate fermentation ($\alpha < 1.055$; Whiticar 1999; Conrad 2005).

Another way to examine these model results involves calculating the DIC-methane isotope separation factor, ε_C, using equation (2). Depth profiles of model-derived values of this quantity agree very well with direct estimates based on our pore-water data (Fig. 2c). Below the SMTZ, both the data and model results converge on a value of around +80‰, which according to Whiticar (1999) is consistent with ε_C values for methanogenesis by CO_2 reduction. As one moves up the sediment column through the SMTZ and into the SO_4^{2-} zone, the calculated isotope separation decreases to ~40‰. Likely explanations for this are twofold. First, isotope fractionation during AOM is much less than it is during methane production, with ε_C values in the literature for AOM generally being less than ~20‰ (e.g., Alperin and Hoehler 2009b). This can also be seen here by the comparatively low model-derived best-fit value of α_{AOM} (1.008; Table 3) versus values of either α_{C2r} or α_{Acf} (~1.100). Second, it is important to remember that in the upper SO_4^{2-} zone of these sediments, oSR, and not AOM or methanogenesis, adds most of the DIC to the pore waters. Therefore, the value calculated here for isotope separation between DIC and methane using equation (2) has little relationship to an ε_C value for methane-DIC fractionation associated with either AOM or methanogenesis and cannot be interpreted in this manner.

The use of either kinetic expression for methanogenesis in the SIRT model results in identical best-fit values of α_{AOM}, 1.008 ± 0.001 (Table 3). This value falls within the range of values determined at other sites with a variety of approaches, including RT models (range 1.004–1.037; e.g., Alperin, Reeburgh, and Whiticar 1988; Martens, Albert, and Alperin 1999; Alperin and Hoehler 2009b; Lloyd, Alperin, and Teske 2011). The range of α_{AOM} values observed at these sites may be related to general site differences, although they may also be related to differences in the way AOM was modeled (or α_{AOM} determined) in each of these studies. Nonetheless, this comparison demonstrates that our value of α_{AOM} agrees well with previously reported estimates of the isotopic fractionation associated with AOM.

6. Discussion

In using these two different kinetic expressions for methanogenesis in the SIRT model, we hypothesized that if these different approaches could be related to the specific processes of CO_2 reduction and acetate fermentation, then only one of the two sets of kinetic expressions would yield reasonable fits to the Santa Barbara Basin sediment isotope data. We also hypothesized that the model results would reveal best-fit values of α_{C2r} and α_{Acf} that could be useful in better understanding the mechanisms of methanogenesis in these sediments. Clearly, the former was not the case (e.g., see Fig. 2), and the latter is somewhat ambiguous because the two α values are virtually identical despite the differences in the two models of methanogenesis.

The similarity between α_{C2r} and α_{Acf} may simply be because of the fact that in and above the SMTZ, oSR and AOM both produce isotopically light DIC — oSR, from remineralization (without fractionation) of POC with an isotopic composition of –20‰ to –21‰, and AOM, which fractionates against $^{13}CH_4$ and produces extremely ^{13}C-depleted DIC from the ^{13}C-depleted CH_4 that diffuses up into the SMTZ (Fig. 2). Together, these two processes drive the isotopic composition of the DIC pool down from a bottom-water value near $\sim$1‰ to a value in the SMTZ and the top of the methanogenic zone that is close to -21‰, which is similar to that of the POC itself (see Table 3). Therefore, mathematically, the factors in equations (16) and (22) that convert rates of methanogenesis (*MP*) to rates of $^{13}CH_4$ production (*MP*13)—namely, the expressions in parentheses on the right sides of these two equations—are likely to be similar in value.

Nevertheless, despite this mathematical ambiguity in the model results, further examination of other model results and measured isotope values suggests that CO_2 reduction is the dominant type of methanogenesis in Santa Barbara Basin sediments. Specifically, the two α values determined with the different models (α_{C2r} and α_{Acf}) are both $\sim$1.100 (see Table 3) and are consistent with those in the literature for methanogenesis by CO_2 reduction (Whiticar 1999; Conrad 2005). The same is true for both measured and model-determined values of ε_C in the methanogenic sediments ($\sim$80%; see Fig. 2c and Section 5). In addition, the suggestion that CO_2 reduction is the predominant type of methanogenesis

in Santa Barbara Basin sediments is also consistent with general observations in the literature discussed in Section 2a. However, we also note that an examination of the hydrogen isotope composition of methane in Santa Barbara Basin sediments would help resolve this uncertainty, given the distinct differences in the fractionation of hydrogen isotopes during methanogenesis by CO_2 reduction versus acetate fermentation (Whiticar 1999; Chanton et al. 2005).

At the same time, a number of other key questions remain regarding the factors controlling the shapes of the isotope depth profiles, as well as their relationship to carbon dynamics in the SMTZ. These are discussed in the following sections.

a. What controls the minimum in $\delta^{13}C_{CH4}$ at the base of the SMTZ?

In addition to Santa Barbara Basin sediments (Fig. 2), minima in $\delta^{13}C_{CH4}$ profiles near the base of the SMTZ have been observed in numerous sedimentary systems (Borowski, Paull, and Ussler 1997; Martens, Albert, and Alperin 1999; Hoehler et al. 2000; Paull et al. 2000; Pohlman et al. 2008; Ussler and Paull 2008; Knab et al. 2009; Hamdan et al. 2011; Henkel et al. 2012; Pohlman et al. 2013; Treude et al. 2014; Yoshinaga et al. 2014). Assuming that these minima occur where there is near-complete consumption of methane, it has been suggested that this feature is inconsistent with conventional isotope systematics (Yoshinaga et al. 2014), presumably because AOM that is responsible for this methane consumption should result in isotopically heavy (and not light) methane being left behind. Several studies have suggested that this minimum may result from what is referred to as "intertwined" AOM and methanogenesis in the SMTZ, in which ^{13}C-depleted DIC produced during AOM is used by methanogens to make ^{13}C-depleted methane (e.g., Borowski, Paull, and Ussler 1997; Pohlman et al. 2008). In contrast, Yoshinaga et al. (2014) recently presented results using sediment enrichment cultures that suggest an alternate explanation for such minima in $\delta^{13}C_{CH4}$ values at the base of the SMTZ (see Section 6a.iii for details).

We examine this problem using Santa Barbara Basin isotope data and model results. First, we suggest that the minimum in the $\delta^{13}C_{CH4}$ depth profile near the base of the SMTZ, at least in Santa Barbara Basin sediments, is consistent with conventional isotope systematics, in part because it can be reproduced by an appropriately parameterized RT model that properly accounts for the fractionation of carbon isotopes during methanogenesis, AOM, and oSR. Furthermore, model results here show that the minimum in $\delta^{13}C_{CH4}$ occurs at methane concentrations of ~1–2 mM (Fig. 3) and not where there is near-complete consumption of methane.

In the next two sections, we further examine this problem first from the perspective of the occurrence and importance of intertwined AOM and methanogenesis in Santa Barbara Basin sediments. We then show that a sharply defined minimum in $\delta^{13}C_{CH4}$ near the base of the SMTZ is more likely the result of an upward flux of methane that is slightly enriched in ^{13}C as compared with the methane in the pore waters of the methanogenic sediments above the lower boundary of the model.

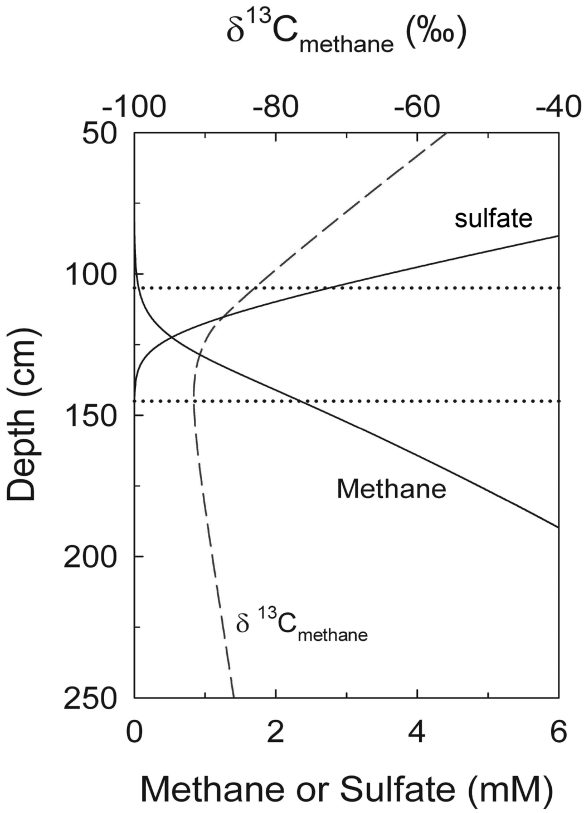

Figure 3. Model-derived depth profiles of pore-water methane, sulfate, and $\delta^{13}C_{CH4}$ (*C2r* model) illustrating that the minimum in $\delta^{13}C_{CH4}$ occurs where sulfate and methane concentrations are both ~0.5–1 and 1–2 mM, respectively (and slightly above the base of the sulfate-methane transition zone [SMTZ]). The model results shown here are taken from Figures 1 and 2 and are plotted on these expanded scales to better illustrate the relationships among these quantities in the SMTZ. Actual data points are not shown here for clarity of presentation. SIRT (stable isotope reaction-transport) model results for $\delta^{13}C_{CH4}$ using the *Acf* kinetic model are also not included here for clarity and because the results in Figure 2 show that they are near identical to the results obtained with the *C2r* kinetic model.

i. Intertwined methanogenesis and AOM In models such as the SIRT model or the OMSN model, different empirical approaches have been used to inhibit the occurrence of less efficient (i.e., lower free-energy yielding) remineralization processes when more efficient (higher free-energy yielding) electron acceptors are present. Here, this specifically involves the inhibition of methanogenesis when sulfate is present above some threshold concentration. Because the rate of AOM is also dependent on the sulfate concentration (equation A1b), this inhibition also impacts how (or even if) AOM and methanogenesis may co-occur in sediments.

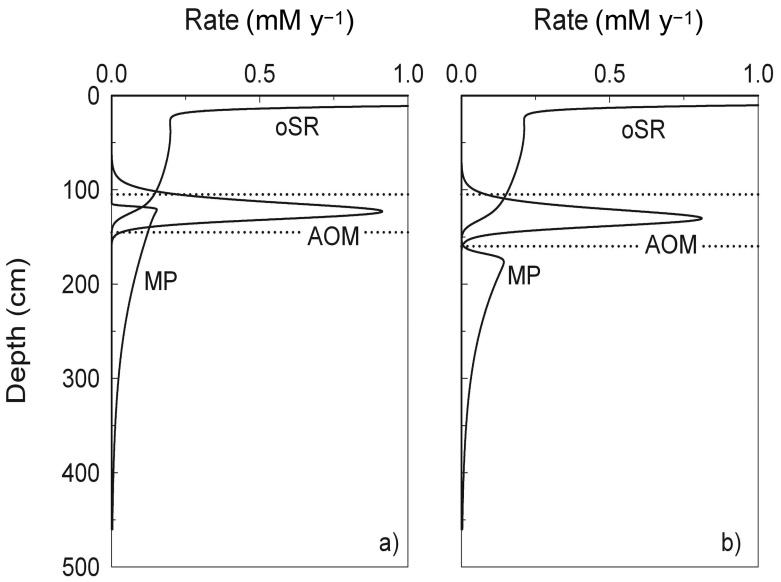

Figure 4. Model-derived depth profiles of the rates of organoclastic sulfate reduction (oSR), anaerobic oxidation of methane (AOM), and methanogenesis (MP). The rate expressions for these three processes are listed in equations (A7), (A1b), and (A1a), respectively, and the depth profiles shown here used these rate expressions and OMSN (organic matter/sulfate/nitrogen) model–derived best-fit parameters and depth profiles of $G_i (i = 1{-}3)$, sulfate (S), and methane (M). The profiles in the left panel (a) used the complementary error function equation (29) for f_S, which allows for the overlap between AOM and MP in the sulfate-methane transition zone. The profiles in the right panel (b) used equation (30) for f_S, which results in effectively no overlap between AOM and MP (see Section 6a.i for more details). Note that the model results in Figures 2–4 were obtained with the same OMSN model results shown here in the left panel.

Mathematically, this inhibition is accomplished in the OMSN and SIRT model equations by multiplying the rate of methanogenesis by the following form of the complementary error function (Martens et al. 1998; Burdige et al. 2016a):

$$f_S = 0.5 \cdot \mathrm{erfc}\left(\frac{S - S*}{K_{\mathrm{in}}}\right) \cong \begin{cases} 1 \; if \; S < S* \\ \\ 0 \; if \; S > S* \end{cases} \tag{29}$$

where K_{in} controls the steepness of the transition of f_S from 0 to 1 that occurs around the sulfate concentration S^* (see, e.g., plots in Martens, Albert, and Alperin 1998). Values for both K_{in} and S^* were obtained during the fitting of the OMSN model to the major solute pore-water data (Burdige et al. 2016a). The best-fit value of S^*, 1.0 $\pm$ 0.2 mM, leads to ~25% of the depth-integrated methanogenesis occurring in the SMTZ (Fig. 4a) and therefore in co-occurrence with AOM.

As discussed previously, model results in Figure 2 that use equation (29) for f_S accurately reproduce the minimum in the $\delta^{13}C_{CH4}$ profile near the base of the SMTZ. However, nearly identical profiles are obtained when we use either the $C2r$ or Acf kinetic expressions for methanogenesis in our RT equations. Because only the $C2r$ kinetic model directly "accesses" the pore-water DIC pool to make methane (compare equations 5 and 6 with equation 20), this suggests that the isotopic composition of DIC in the pore waters, and therefore production of isotopically light DIC by AOM, does not play a major role in explaining this observed minimum in $\delta^{13}C_{CH4}$ near the base of the SMTZ. It therefore also implies that intertwined AOM and methanogenesis may not necessarily be required to explain this feature in the $\delta^{13}C_{CH4}$ profile.

To further examine this problem, we used a slightly different formulation for f_S in which the inhibition function transitions from 0 to 1 effectively at 0 mM sulfate. This equation,

$$f_S = \frac{10^{-5}}{S + 10^{-5}}, \tag{30}$$

was also used in our earlier modeling studies (Burdige and Komada 2011). Fitting the Santa Barbara Basin inorganic pore-water data to a modified version of the OMSN model with the equation (30) version of f_S results in there being effectively no overlap between AOM and methanogenesis (Fig. 4b). Best-fit model-derived pore-water profiles for DIC, sulfate, and methane using the equation (30) version of f_S (not shown here) are extremely similar to those in Figure 1, which use the equation (29) version of f_S. Relative root-mean-square differences between the pairs of best-fit results for each of these solutes is $<2\%$, as is also the case for the pair of model-derived profiles of total reactive organic carbon (i.e., G_t in Fig. 1). Model-derived best-fit parameters obtained with models using either version of f_S agree with one another within 1 standard deviation (results not shown here).

Using this new OMSN model fit to refit the SIRT model to the isotope data (Fig. 5), we see that a more strict separation of AOM and methanogenesis in the SMTZ has a minor impact on the model-derived best-fit to the $\delta^{13}C_{CH4}$ data, although model results using equation (29) for f_S do a slightly better job of capturing the sharpness in the minimum in $\delta^{13}C_{CH4}$ at the base of the SMTZ as compared with model results obtained using equation (30) for f_S. A similar comparison also shows that the choice of f_S has little impact on model fits to the $\delta^{13}C_{DIC}$ results. Similarly, when the best-fit SIRT model parameters ($\delta_1, \delta_2, \ldots, \delta_{JlbM}, \delta_{JlbD}$) obtained using equation (29) for f_S (Table 3) are compared with the equivalent values obtained with model fits using equation (30) for f_S (results not shown here), the comparison indicates that with the exception of α_{AOM}, the pairs of individual values all agree with one another to within 1 standard deviation. The α_{AOM} values differed by 0.004 with each pair of values having uncertainties of 0.001.

In summary then, given the different ways that equations (29) and (30) impact the overlap of AOM and methanogenesis in the SMTZ, these results further indicate that intertwined AOM and methanogenesis is not necessarily required to explain the minimum in $\delta^{13}C_{CH4}$ observed at the base of the SMTZ.

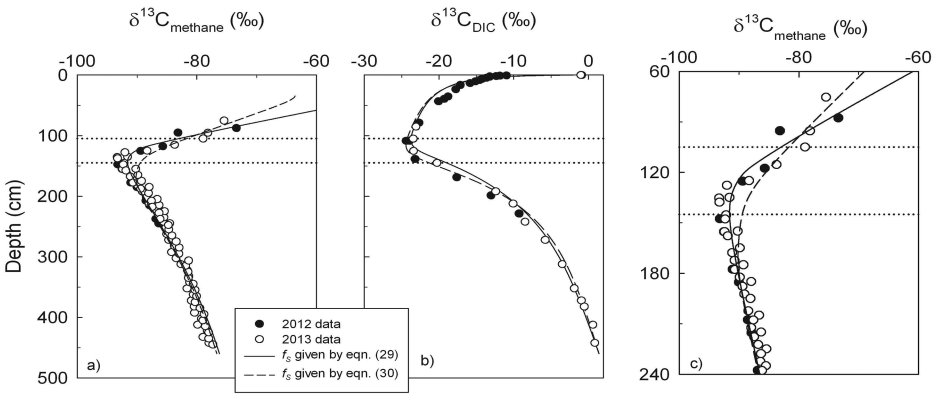

Figure 5. Depth profiles of pore-water $\delta^{13}C_{CH4}$ (a and c; expanded view of the sulfate-methane transition zone region) and $\delta^{13}C_{DIC}$ (b) in Santa Barbara Basin sediments (data from Komada et al. 2016), along with best fits of the SIRT (stable isotope reaction-transport) model (using the $C2r$ kinetic model for methanogenesis) to the data. One of the two model fits was obtained with OMSN (organic matter/sulfate/nitrogen) model results that used equation (29) for f_S (solid lines), and the other was obtained using equation (30) for f_S (dashed lines). Analogous model results with the *Acf* kinetic model for methanogenesis show similar comparative results and are not shown here for clarity of presentation. Note that the model results shown here that used equation (29) for f_S are the same as those in Figure 2.

ii. The role of upward basal fluxes The model results presented here (Fig. 2 and Table 3) suggest that an upward basal flux of methane slightly enriched in ^{13}C as compared with the ambient pore waters may be the reason why we observe a sharply defined minimum in $\delta^{13}C_{CH4}$ near the base of the SMTZ. To more directly test this suggestion, we first attempted to refit the OMSN model to the major solute data assuming that the methane and DIC basal fluxes were equal to zero and then used these results to reexamine the methane and DIC isotope profiles with the SIRT model.

This approach (Fig. 6) yields a fit to the sulfate data that is virtually indistinguishable from the fit in Figure 1, in which there are nonzero basal DIC and methane diffusive fluxes. The fits to the methane data with either type of lower boundary condition are not significantly different from one another above ∼150 cm, although below this depth the model fit with no basal flux approaches an asymptotic concentration at depth of ∼12 mM. In contrast, the original fit (Fig. 2) continues to increase linearly with depth because of the presence of an upward basal methane flux. The two fits to the DIC data are in good agreement above the SMTZ, although the fits result in slightly different DIC concentrations at depth because of the presence/absence of a DIC basal flux.

Using the results in Figure 6, we then fit the SIRT model to the isotope data, and this is shown in Figure 7. With no basal DIC and methane fluxes, best-fit solutions of the SIRT model to the $\delta^{13}C_{DIC}$ data using either kinetic model of methanogenesis reproduce the general shape of the profile and are not significantly different than the model results

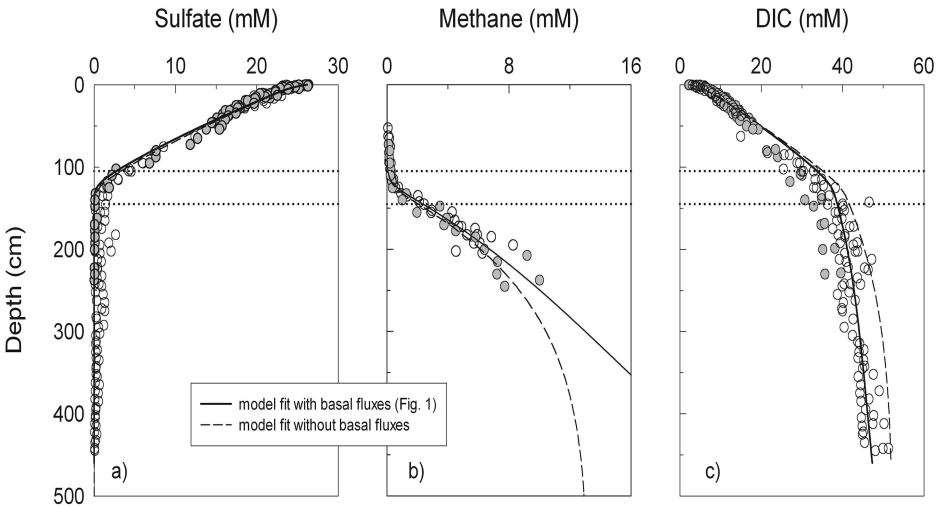

Figure 6. Depth profiles of pore-water sulfate (a), methane (b), and dissolved inorganic carbon (DIC) (c) concentrations in Santa Barbara Basin sediments (data from Komada et al. 2016), along with the best-fit of the OMSN (organic matter/sulfate/nitrogen) model to the data (Burdige et al. 2016a) assuming nonzero methane and DIC basal fluxes (solid lines), and zero methane and DIC basal fluxes (dashed lines; see Section 6a.ii for details). Note that the model results shown here with nonzero basal fluxes are the same as those in Figure 1.

in Figure 2, which include basal DIC and methane fluxes. This likely occurs because the addition of isotopically enriched (heavy) DIC during methanogenesis, as evidenced by the positive ε_C value observed here (= 80%; see equation 2), causes the $\delta^{13}C_{DIC}$ profile to turn around from the very negative $\delta^{13}C$ values for the DIC in the SMTZ. The resulting minimum in the $\delta^{13}C_{DIC}$ profile is therefore somewhat independent of the isotopic composition of the basal DIC flux, which appears to have a minor impact on the shape of the $\delta^{13}C_{DIC}$ profile.

In contrast, the absence of a basal methane flux in solutions of the SIRT model using either kinetic model of methanogenesis fails to reproduce the shape of the $\delta^{13}C_{CH4}$ profile (Fig. 7a). With the *Acf* kinetic model, $\delta^{13}C_{CH4}$ is essentially invariant with depth below the SMTZ, and using the *C*2*r* kinetic model, $\delta^{13}C_{CH4}$ only goes through a small (∼3‰–4‰) minimum below the SMTZ. However, neither of these results accurately reproduces the shape of the $\delta^{13}C_{CH4}$ methane profile as compared with the results in Figure 2. Because methanogenesis produces extremely isotopically depleted (light) methane, in the absence of an upward basal flux of relatively ^{13}C-enriched methane, $\delta^{13}C_{CH4}$ remains low and roughly invariant with depth below the SMTZ. In contrast, an upward flux of relatively ^{13}C-enriched methane then results in the observed sharp minimum (turn around) in the $\delta^{13}C_{CH4}$ profile near the base of the SMTZ. Possible sources of this methane are discussed in Section 6b.

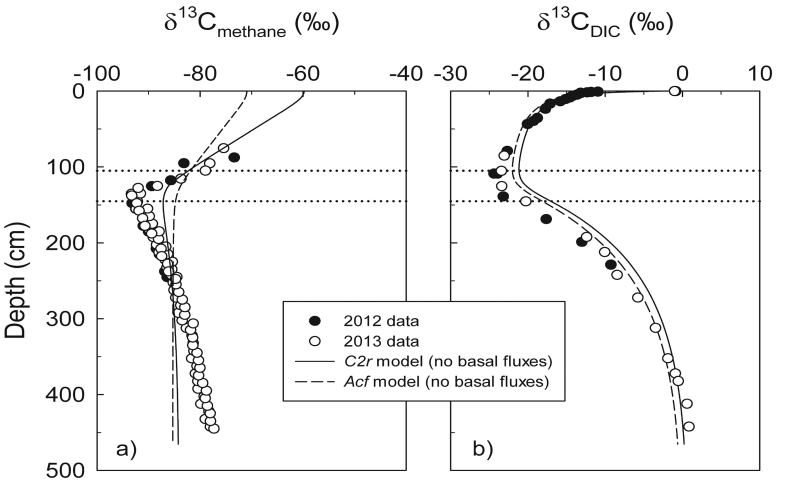

Figure 7. Depth profiles of pore-water $\delta^{13}C_{CH4}$ (a) and $\delta^{13}C_{DIC}$ (b) in Santa Barbara Basin sediments (data from Komada et al. 2016), along with "fits" of the SIRT (stable isotope reaction-transport) model to the data (using both kinetic expressions for methanogenesis) based on OMSN (organic matter/sulfate/nitrogen) model results with zero methane and dissolved inorganic carbon (DIC) basal fluxes (see Fig. 6).

iii. Carbon isotope equilibration as a possible explanation for minima in $\delta^{13}C_{CH4}$ *at the base of the SMTZ* In a recent study, Yoshinaga et al. (2014) showed that carbon isotope equilibration between methane and DIC occurred during sulfate-limited AOM with enrichment cultures isolated from methane seep surface sediments on Hydrate Ridge (northeast Pacific Ocean) and from Amon Mud Volcano (eastern Mediterranean). They further argued that this phenomenon may be a better explanation for minima in $\delta^{13}C_{CH4}$ pore-water profiles near the base of the SMTZ than coupled (intertwined) AOM and methanogenesis in the SMTZ. We too have shown that coupled AOM and methanogenesis is not required to explain this feature in pore-water $\delta^{13}C_{CH4}$ profiles (Section 6a.i). However, our results also suggest that this type of isotope equilibration may not be required to explain this feature, because the type of isotope equilibration they observed is not included in the SIRT model as it is currently formulated.

Related to this suggestion, Alperin and Hoehler (2009a) highlighted some of the differences between what they termed "classical" and "nouveau" AOM environments. Based on their classification, Santa Barbara Basin sediments would clearly be considered a diffusion-controlled "classical" AOM setting, whereas the sediments studied by Yoshinaga et al. (2014) would be considered fluid advection- and/or ebullition-controlled "nouveau" settings. Given some of the differences between these types of AOM environments discussed by Alperin and Hoehler (2009a), it seems likely that these differences might also explain why our model can successfully reproduce a minimum in the pore-water $\delta^{13}C_{CH4}$ profile

near the base of the SMTZ without incorporating into the model equations carbon isotope equilibration between methane and DIC during AOM. We also note that many of the other sites where such minima in $\delta^{13}C_{CH4}$ profiles occur (see references at the beginning of Section 6a) would also be classified as "classical" (diffusion-controlled) AOM settings. Thus, the significance of an upward methane flux as an explanation for this minimum in $\delta^{13}C_{CH4}$ pore-water profiles may not be limited to Santa Barbara Basin sediments but may also be applicable to other "classical" AOM sites, and the type of isotope equilibration observed by Yoshinaga et al. (2014) may not occur universally in all aquatic systems where AOM occurs.

b. The source(s) of deep methane fluxes

In light of these observations, the question then is: What is the source of this deep methane flux? One possibility is a "deep" geologic hydrocarbon reservoir derived from ancient source rocks or the decomposition of buried gas hydrate deposits. Buried gas hydrates and gas deposits are common in many continental margin settings (Bohrmann and Torres 2006), including the California Borderland region in general and Santa Barbara Basin in particular (Hill, Kennett, and Spero 2004; Hein et al. 2006; Leifer et al. 2006; Normark, Piper, Sliter 2006; Paull et al. 2008). However, a second source of this methane may be biogenic (or perhaps thermogenic) methane produced hundreds of meters below the seafloor. This type of methane production is common in outer continental margin/continental slope sediments and appears to be stimulated by increasing sediment temperatures associated with the sediment geothermal gradient (i.e., from bottom-water temperatures of ~2°C–3°C to up to ~100°C–120°C; Wellsbury et al. 1997; Parkes et al. 2007; Burdige 2011).

Following up on earlier work examining this problem (Burdige et al. 2016a), we note here that the $\delta^{13}C$ of the basal methane flux (–64‰ to –68‰; see Table 3) is heavier than that of the methane in Santa Barbara Basin pore waters but is still within the range observed for biogenic methane (Whiticar 1999). This then does not eliminate either of these two deep methane sources because much of the methane found in gas hydrates and gas deposits is ultimately biogenic in origin (Bohrmann and Torres 2006).

The methane in deep Santa Barbara Basin sediment pore waters (below 4 m) has a $\Delta^{14}C$ value of almost –600‰ (Komada et al. 2016), and thus the $\Delta^{14}C$ content of the upward methane flux is also expected to be extremely depleted in radiocarbon. This observation does not eliminate any of the possible deep methane sources discussed at the beginning of this section. The positive $\delta^{13}C$ value of the DIC flux (~70‰; see Table 3) suggests that this DIC could also be derived from deep methanogenesis. However, the ratio of the methane to DIC basal flux (4.5; see results in Table A1 in the Appendix) argues against this because such a deep biogenic source should result in a flux ratio closer to 1, based on the stoichiometry of methanogenesis in equation (1).

Unfortunately, the results presented here do not provide any clear insights into the processes that lead to this upward basal flux of methane (and DIC) in Santa Barbara

Bain sediments. Earlier attempts to answer this question based solely on examining the magnitudes of the observed methane, DIC, and ammonium basal fluxes were similarly equivocal (Burdige et al. 2016a). Nevertheless, minima in $\delta^{13}C_{CH4}$ profiles near the base of the SMTZ have been seen in a wide range of other sedimentary systems beyond Santa Barbara Basin sediments (see references at the beginning of this section) illustrating the importance of active methanogenesis and upward fluxes of methane from deeper sources in controlling carbon dynamics and isotopic signatures in the SMTZ of such sediments.

At the same time, these observations further indicate the effectiveness of methane consumption by AOM in the SMTZ as a barrier for the escape of this deep methane from continental margin sediments to the water column and perhaps the atmosphere. This barrier is of importance because the size of the gas hydrate methane reservoir, though not well constrained, is significant, perhaps as large as 15,000 Gt C (Archer 2007). For comparison, this value is comparable to the global inventory of all other fossil fuels (which also includes methane found in known gas deposits).

Because methane is a powerful greenhouse gas, understanding the factors that control this sedimentary barrier to the release of methane trapped in continental margin gas hydrates is important for addressing questions about past changes in methane cycling that may have affected global temperatures (see discussions in Berner 2004; Payne et al. 2004; Dickens 2011; Gu et al. 2011). It is also important in examining how the effect of rising bottom-water temperatures and deoxygenation (two likely outcomes of anthropogenic global warming; Keeling, Körtzinger, and Gruber 2009; Houghton 2015) will impact this barrier. Although the impact of the potential release of this methane on future climate may take several millennia (Archer 2007), such a methane release still has the possibility to act as a more long-term positive feedback on anthropogenic climate change.

7. Summary and conclusions

A new RT model for $\delta^{13}C_{CH4}$ and $\delta^{13}C_{DIC}$ in the anoxic sediments is described. The model was successfully applied to pore-water profiles of these isotope signatures in Santa Barbara Basin sediments. Specifically, best-fit solutions of the model to these data accurately reproduce the broad minimum in the $\delta^{13}C_{DIC}$ depth profile and the much sharper (angular) minimum in the $\delta^{13}C_{CH4}$ depth profile, both of which are seen near the base of the SMTZ. Such minima in $\delta^{13}C_{CH4}$ profiles near the base of the SMTZ are not unique to Santa Barbara Basin sediments and have also been observed in other sedimentary systems. These results also suggest that CO_2 reduction is the predominant form of methanogenesis in Santa Barbara Basin sediments.

Based on these model results, this minimum in the $\delta^{13}C_{CH4}$ profile in Santa Barbara Basin sediments results from the balance between (1) AOM, which leads to an increase in $\delta^{13}C_{CH4}$ with decreasing depth in the sediment column through and above the SMTZ; (2) methanogenesis, which produces ^{13}C-depleted methane, both in and below the SMTZ;

and (3) an upward flux of CH_4 from depth that is relatively enriched in ^{13}C as compared with the methane in the pore waters within the model domain.

Other explanations in the literature for minima in $\delta^{13}C_{CH4}$ pore-water profiles near the base of the SMTZ include the co-occurrence of (or intertwined) AOM and methanogenesis, as well as carbon isotope equilibration between methane and DIC during sulfate-limited AOM. Our results demonstrate that intertwined AOM and methanogenesis is not necessary to explain this feature in the $\delta^{13}C_{CH4}$ profile, and that the feature also does not require methane-DIC isotope exchange during sulfate-limited AOM. We further suggest that the significance of an upward methane flux as an explanation for this minimum in $\delta^{13}C_{CH4}$ pore-water profiles near the base of the SMTZ may not be limited to Santa Barbara Basin sediments.

Possible sources of this deep methane include the following: geologic hydrocarbon reservoirs derived from ancient source rocks or the decomposition of buried gas hydrate deposits, or biogenic (or perhaps thermogenic) methane produced hundreds of meters below the seafloor stimulated by increasing temperatures associated with the sediment geothermal gradient. Unfortunately, with existing data we are unable to differentiate between the occurrences of these possible deep methane sources.

These results illustrate the importance, in general, of active methanogenesis and upward fluxes of methane from deeper sources in controlling carbon dynamics in the SMTZ. They further indicate the effectiveness of the SMTZ as a barrier for the escape of this deep methane from continental margin sediments into the water column and perhaps into the atmosphere. Understanding these dynamics is important for addressing questions about past changes in methane cycling that may have affected global temperatures, as well as for how rising bottom-water temperatures and deoxygenation, two likely outcomes of anthropogenic global warming, may impact this barrier.

Acknowledgments. This work was supported by the following grants from the U.S. National Science Foundation: OCE-1155562 (DJB), OCE-1155764 (TK), and OCE-1155320 (JPC). We thank Bernie Boudreau, Andy Dale, and Associate Editor Bob Aller for useful comments that greatly improved an earlier version of this manuscript.

APPENDIX

a. Reaction transport (RT) equations in the stable isotope reaction-transport (SIRT) model

i. RT equation for methane

$$\frac{\partial M}{\partial t} = \frac{1}{\varphi}\frac{\partial}{\partial z}\left(\varphi D_s \frac{\partial M}{\partial z}\right) - \frac{1}{\varphi}\frac{\partial}{\partial z}(\varphi v M) - AOMr + MP \tag{A1}$$

The terms on the right side of this equation represent diffusion, advection driven by sedimentation and compaction, and the rate expressions for anaerobic oxidation of methane (*AOMr*) and methane production (*MP*), where

$$MP = f_s\,\Im L_2 \sum_{i=1}^{3} k_i G_i \tag{A1a}$$

$$AOMr = \frac{k_{\mathrm{aom}} SM}{K_a + S}. \tag{A1b}$$

Analogous diffusion and advection terms also appear in the remaining equations shown subsequently. Equation (A1) is taken from the OMSN (organic matter/sulfate/nitrogen) model (Burdige et al. 2016a). All variables and parameters used in these model equations are defined in Table 1.

ii. RT equation for $^{13}CH_4$ (CO_2 reduction model [C2r] model)

$$\frac{\partial M13}{\partial t} = \frac{1}{\varphi}\frac{\partial}{\partial z}\left(\varphi D_s \frac{\partial M13}{\partial z}\right) - \frac{1}{\varphi}\frac{\partial}{\partial z}\left(\varphi v M13\right) - \left(\frac{M13}{\alpha_{\mathrm{AOM}} M - (\alpha_{\mathrm{AOM}} - 1) M13}\right) AOMr + MP13_{\mathrm{C2r}} \tag{A2}$$

The reaction terms on the right side of this equation represent $^{13}CH_4(M13)$ consumption by AOM and $^{13}CH_4$ production in the *C2r* model ($MP13_{\mathrm{C2r}}$), which is given by

$$MP13_{C2r} = \left(\frac{D13}{\alpha_{\mathrm{C2r}} D - (\alpha_{\mathrm{C2r}} - 1) D13}\right) f_s\ \Im\ L_2 \sum_{i=1}^{3} k_i G_i. \tag{A2a}$$

iii. RT equation for $^{13}CH_4$ (acetate fermentation [Acf] model)

$$\frac{\partial M13}{\partial t} = \frac{1}{\varphi}\frac{\partial}{\partial z}\left(\varphi D_s \frac{\partial M13}{\partial z}\right) - \frac{1}{\varphi}\frac{\partial}{\partial z}\left(\varphi v M13\right) - \left(\frac{M13}{\alpha_{\mathrm{AOM}} M - (\alpha_{\mathrm{AOM}} - 1) M13}\right) AOMr + MP13_{\mathrm{Acf}} \tag{A3}$$

In equation (A3), the reaction terms on the right side of the equation represent $^{13}CH_4$ consumption by AOM and $^{13}CH_4$ production in the Acf model ($MP13_{\mathrm{Acf}}$), the latter of which is given by

$$MP13_{\mathrm{Acf}} = f_s \Im L_2 \sum_{i=1}^{3} \frac{r_{\mathrm{Gi}}^{13}}{\alpha_{\mathrm{Acf}} - r_{\mathrm{Gi}}^{13}(\alpha_{\mathrm{Acf}} - 1)} k_i G_i. \tag{A3a}$$

iv. RT equation for dissolved inorganic carbon (DIC)

$$\frac{\partial D}{\partial t} = \frac{1}{\varphi}\frac{\partial}{\partial z}\left(\varphi D_s \frac{\partial D}{\partial z}\right) - \frac{1}{\varphi}\frac{\partial}{\partial z}\left(\varphi v D\right) + \Im \sum_{i=1}^{3} \frac{k_i G_i S}{K_m + S} + DMP + AOMr - ACP(z) \tag{A4}$$

The reaction terms on the right side of this equation represent DIC production by organoclastic sulfate reduction (oSR) and methanogenesis (*DMP*), DIC production by AOM, and DIC consumption by authigenic carbonate precipitation, *ACP*(z) (see Equation A9) where

$$DMP = f_s\,\Im L_3 \sum_{i=1}^{3} k_i G_i. \tag{A4a}$$

Equation (A4) is taken from the OMSN model (Burdige et al. 2016a). The depth distribution of authigenic carbonate precipitation, *ACP*(z), used here and in the OMSN model equations was obtained by fitting the RT equation for Ca^{2+} (in the OMSN model) to the Ca^{2+} porewater data assuming that the rate of authigenic carbonate precipitation rate can be described using a Gaussian function of depth (for more details, see Table A1 and Burdige et al. 2016a).

v. RT equation for DI ^{13}C (C2r model)

$$\frac{\partial D13}{\partial t} = \frac{1}{\varphi}\frac{\partial}{\partial Z}\left(\varphi D_s \frac{\partial D13}{\partial Z}\right) - \frac{1}{\varphi}\frac{\partial}{\partial Z}(\varphi v D13) + \Im \sum_{i=1}^{3} \frac{k_1\, r_{\mathrm{Gi}}^{13} G_i S}{K_m + S} + DMP13_{\mathrm{C2r}} + \left(\frac{M13}{\alpha_{\mathrm{AOM}} M - (\alpha_{\mathrm{AOM}} - 1) M13}\right) AOMr - \left(\frac{D13}{D}\right) ACP(z) \tag{A5}$$

The reaction terms on the right side of this equation represent DI^{13}C ($D13$) production by oSR and methanogenesis ($DMP13_{\mathrm{C2r}}$), DI^{13}C production by AOM, and DI^{13}C consumption by authigenic carbonate precipitation, where

$$DMP13_{\mathrm{C2r}} = f_s \Im \sum_{i=1}^{3} k_i\, r_{\mathrm{Gi}}^{13}\, G_i - \left(\frac{D13}{\alpha_{\mathrm{C2r}} D - (\alpha_{\mathrm{C2r}} - 1) D13}\right) f_s \Im L_2 \sum_{i=1}^{3} k_i G_i. \tag{A5a}$$

vi. RT equation for DI^{13}C (Acf model)

$$\frac{\partial D13}{\partial t} = \frac{1}{\varphi}\frac{\partial}{\partial Z}\left(\varphi D_s \frac{\partial D13}{\partial Z}\right) - \frac{1}{\varphi}\frac{\partial}{\partial Z}(\varphi v D13) + \sum_{i=1}^{3} \frac{k_i\ \Im r_{\mathrm{Gi}}^{13} G_i S}{K_m + S} + DMP13_{\mathrm{Acf}} + \left(\frac{M13}{\alpha_{\mathrm{AOM}} M - (\alpha_{\mathrm{AOM}} - 1) M13}\right) AOMr - \left(\frac{D13}{D}\right) ACP(z) \tag{A6}$$

The reaction terms on the right side of this equation represent DI^{13}C ($D13$) production by oSR and methanogenesis ($DMP13_{\mathrm{Acf}}$), DI^{13}C production by AOM, and DI^{13}C consumption by authigenic carbonate precipitation, where

$$DMP13_{\mathrm{Acf}} = f_s \Im \sum_{i=1}^{3} k_i\, r_{\mathrm{Gi}}^{13}\, G_i - f_s \Im \sum_{i=1}^{3} \frac{r_{\mathrm{Gi}}^{13}}{\alpha_{\mathrm{Acf}} - (\alpha_{\mathrm{Acf}} - 1) r_{\mathrm{Gi}}^{13}} L_2 k_i G_i. \tag{A6a}$$

Table A1. The best-fit parameters obtained by fitting the OMSN (organic matter/sulfate/nitrogen) model to the major solute data (from Burdige et al. 2016a).

Parameter[a]	Bestfit value[b]	Units
G_1^o	0.86 ± 0.16	wt%
G_2^o	0.64 ± 0.26	wt%
G_3^o	0.64 ± 0.07	wt%
k_1	0.54 ± 0.10	y^{-1}
k_2	0.17 ± 0.04	y^{-1}
k_3	$2.5 \pm 1.0 \times 10^{-3}$	y^{-1}
k_{aom}	4.98 ± 1.50	y^{-1}
J_{lbM}[c]	-0.243 ± 0.059	mmol m^{-2} d^{-1}
J_{lbD}[c]	-0.054 ± 0.016	mmol m^{-2} d^{-1}
J_{lbC}[c]	0.007	mmol m^{-2} d^{-1}
K_{in}[d]	0.20 ± 0.04	mM
S^{*}[d]	0.98 ± 0.16	mM
R_{max}[e]	0.064	mM y^{-1}
z_{cp}[e]	41.4	cm
s_{cp}[e]	84.7	cm

Notes: [a] Except where noted, see Table 1 for parameter definitions. [b] All errors are 1 standard deviation. [c] Basal fluxes of methane (subscript M), dissolved inorganic carbon (subscript D), and Ca^{2+} (subscript C). [d] See equation 29. [e] The best-fit values of the Gaussian function used to define the depth distribution of authigenic carbonate precipitation, $ACP(z)$ (for details, see Burdige et al. 2016a):

$$ACP(z) = R_{max} e^{-0.5[(z_{cp}-z)/s_{cp}]^2}. \tag{A9}$$

vii. RT equation for sulfate

$$\frac{\partial S}{\partial t} = \frac{1}{\varphi}\frac{\partial}{\partial z}\left(\varphi D_s \frac{\partial S}{\partial z}\right) - \frac{1}{\varphi}\frac{\partial}{\partial z}\left(\varphi v S\right) - \sum_{i=1}^{3} \frac{k_i L_2 \Im G_i S}{K_m + S} - AOMr \tag{A7}$$

The reaction terms on the right hand side of this equation represent sulfate consumption by oSR and AOM. Equation (A7) is taken from the OMSN model (Burdige et al. 2016a).

viii. RT equation for G_i

$$\frac{\partial G_i}{\partial t} = -\frac{1}{1-\varphi}\frac{\partial}{\partial z}[\omega(1-\varphi)G_i] - \frac{k_i G_i S}{K_m + S} - f_S k_i G_i \tag{A8}$$

The terms on the right side of this equation represent advection driven by sediment burial (sedimentation), oSR, and methanogenesis. These three G_i fractions are a subset of the total sediment particulate organic carbon (POC) pool, which also includes a "refractory" component that is nonmetabolizable over the time and depth scale of the model domain. Equation (A8) is taken from the OMSN model (Burdige et al. 2016a).

b. Solution of the SIRT model equations

To solve the SIRT model equations for $M13$ and $D13$ (see equations A2–A5), we expanded the spatial derivatives in the advective and diffusive terms in the equations as described previously (Burdige et al. 2016a). For a general solute C, this implies that

$$\begin{aligned}\frac{\partial C}{\partial t} &= \frac{1}{\varphi}\frac{\partial}{\partial z}\left(\varphi D_s \frac{\partial C}{\partial z}\right) - \frac{1}{\varphi}\frac{\partial}{\partial z}(\varphi v C) + \cdots \\ &= D_s \frac{\partial^2 C}{\partial x^2} + \frac{D^o}{\varphi}\frac{\partial f}{\partial x}\frac{\partial C}{\partial x} - \frac{W}{\varphi}\frac{\partial C}{\partial x} + \cdots, \\ &= D_s \frac{\partial^2 C}{\partial x^2} + \left(\frac{D^o}{\varphi}\frac{\partial f}{\partial x} - \frac{W}{\varphi}\right)\frac{\partial C}{\partial x} + \cdots\end{aligned} \tag{A10}$$

where "…" represents the reaction terms in each equation, $D^o = D_s/\theta^2$,

$$f = \frac{\varphi}{\theta^2} = \frac{\varphi}{1 - 2\ln(\varphi)} \tag{A11}$$

(see Table 1), and

$$W = \frac{\varphi_\infty F_{\text{sed}}}{\rho_{\text{ds}}(1 - \varphi_\infty)} \tag{A12}$$

(also see equations 6.15–6.19 in Burdige 2006, and note the W/φ has units of sediment burial, e.g., cm y^{-1}). Porosity is also a function of depth in these sediments and is expressed as

$$\varphi(z) = 0.78 + 0.07e^{-0.174z} + 0.15e^{-0.006z} \tag{A13}$$

(see Komada et al. 2016, for details).

After expansion of these derivatives, the model equations were solved numerically using the method of lines technique with variable grid spacing (Schiesser 1991; Boudreau 1997; Burdige et al. 2016a). A centered-finite differencing scheme was used to approximate the first and second spatial derivatives in the equations (Boudreau 1997). With this approach, the RT equations for $M13$ and $D13$ were transformed from space- and time-dependent partial differential equations into sets of n time-dependent ordinary differential equations (ODEs) for each solute valid at each grid point of the model domain (note that n is the total number of grid points). To obtain steady-state solutions of these equations, these time-dependent

ODEs are solved in MATLAB using the integration package *ode15s*, and the model is run for a long enough time period that steady-state conditions are reached (Boudreau 1996; Burdige 2011).

In the set of ODEs for each solute, the upper boundary condition is satisfied by setting the time-dependent ODE at the first grid point ($z = 0$ cm) equal to zero, with the bottom-water concentration then specified as the $z = 0$ cm value in the initial condition of the model solution (also see Hamdi, Schiesser, and Griffiths 2007). At the lower boundary (i.e., at the nth grid point), a flux boundary condition is used (see Section 3b). This boundary condition is implemented by first using a slightly different numerical approximation of the second spatial derivative (other than centered-finite differencing), to avoid "imaginary" concentrations and grid points outside of the model domain (Boudreau 1997). Defining the diffusive flux (J_{lb}) at the boundary condition as

$$J_{\mathrm{lb}} = -\varphi_n D_s \left.\frac{\partial C}{\partial z}\right|_n, \tag{A14}$$

this second derivative can be written as

$$\left.\frac{\partial^2 C}{\partial x^2}\right|_n = \frac{2}{\Delta z_n^2}\left(C_{n-1} - C_n - \frac{J_{\mathrm{lb}}\Delta z_n}{\varphi_n D_s}\right), \tag{A15}$$

and equations (A14) and (A15) can be substituted into the numerical version of equation (A10) at the lower boundary as

$$\left.\frac{dC}{dt}\right|_n = \frac{2D_s}{\Delta z_n^2}\left(C_{n-1} - C_n - \frac{J_{\mathrm{lb}}\Delta z_n}{\varphi_n D_s}\right) - \left(\frac{D^o}{\varphi_n}\left.\frac{\partial f}{\partial z}\right|_n - \frac{W}{\varphi_n}\right)\left(\frac{J_{\mathrm{lb}}}{\varphi_n D_s}\right). \tag{A16}$$

REFERENCES

Alperin, M. J., N. E. Blair, D. B. Albert, T. M. Hoehler, and C. S. Martens. 1992. Factors that control the stable carbon isotopic composition of methane produced in an anoxic marine sediment. Global Biogeochem. Cycles, *6*(3), 271–291. doi: 10.1029/92GB01650

Alperin, M. J., and T. M. Hoehler. 2009a. Anaerobic methane oxidation by archaea/sulfate-reducing bacteria aggregates: 1. Thermodynamic and physical constraints. Am. J. Sci., *309*(10), 869–957. doi: 10.2475/10.2009.01

Alperin, M. J., and T. M. Hoehler. 2009b. Anaerobic methane oxidation by archaea/sulfate-reducing bacteria aggregates: 2. Isotopic constraints. Am. J. Sci., *309*(10), 958–984. doi: 10.2475/10.2009.02

Alperin, M. J., W. S. Reeburgh, and M. J. Whiticar. 1988. Carbon and hydrogen isotopic fractionation resulting from anaerobic methane oxidation. Global Biogeochem. Cycles, *2*(3), 279–288. doi: 10.1029/GB002i003p00279

Archer, D. 2007. Methane hydrate stability and anthropogenic climate change. Biogeosciences, *4*(4), 521–544. doi: 10.5194/bg-4-521-2007

Archer, D. E., B. A. Buffett, and P. C. McGuire. 2012. A two-dimensional model of the passive coastal margin deep sedimentary carbon and methane cycles. Biogeosciences, *9*(8), 2859–2878. doi: 10.5194/bg-9-2859-2012

Arning, E. T., W. van Berk, and H.-M. Schulz. 2016. Fate and behaviour of marine organic matter during burial of anoxic sediments: Testing CH_2O as generalized input parameter in reaction transport models. Mar. Chem., *178*, 8–21. doi: 10.1016/j.marchem.2015.12.002

Berelson, W. M., M. Prokopenko, F. J. Sansone, A. W. Graham, J. McManus, and J. M. Bernhard. 2005. Anaerobic diagenesis of silica and carbon in continental margin sediments: Discrete zones of TCO_2 production. Geochim. Cosmochim. Acta, *69*(19), 4611–4629. doi: 10.1016/j.gca.2005.05.011

Berner, R. A. 1980. Early Diagenesis: A Theoretical Approach. Princeton, NJ: Princeton University Press.

Berner, R. A. 2004. The Phanerozoic Carbon Cycle. Oxford: Oxford University Press.

Blair, N. 1998. The $\delta^{13}C$ of biogenic methane in marine sediments: The influence of C_{org} deposition rate. Chem. Geol., *152*(1–2), 139–150. doi: 10.1016/S0009-2541(98)00102-8

Blair, N. E., S. E. Boehme, and W. D. Carter, Jr. 1993. The carbon isotope biogeochemistry of methane production in anoxic sediments: 1. Field observations, *in* Biogeochemistry of Global Change, R. S. Oremland, ed. New York: Chapman & Hall, 574–593.

Blair, N. E., C. S. Martens, and D. J. DesMarais. 1987. Natural abundances of carbon isotopes in acetate from from a coastal marine sediment. Science, *236*(4797), 66–68. doi: 10.1126/science.11539717

Boehme, S. E., N. E. Blair, J. P. Chanton, and C. S. Martens. 1996. A mass balance of ^{13}C and ^{12}C in an organic-rich methane-producing marine sediment. Geochim. Cosmochim. Acta, *60*(20), 3835–3848. doi: 10.1016/0016-7037(96)00204-9

Bohrmann, G., and M. E. Torres. 2006. Gas hydrates in marine sediments, *in* Marine Geochemistry, H. D. Schultz and M. Zabel, eds. Berlin: Springer, 481–512.

Borowski, W. S., C. K. Paull, and W. Ussler III. 1997. Carbon cycling within the upper methanogenic zone of continental rise sediments: An example from the methane-rich sediments overlying the Blake Ridge gas hydrate deposits. Mar. Chem., *57*(3–4), 299–311. doi: 10.1016/S0304-4203(97)00019-4

Boudreau, B. P. 1996. A method-of-lines code for carbon and nutrient diagenesis in aquatic sediments. Comput. Geosci., *22*(5), 479–496. doi: 10.1016/0098-3004(95)00115-8

Boudreau, B. P. 1997. Diagenetic Models and Their Implementation. Berlin: Springer-Verlag.

Burdige, D. J. 2006. Geochemistry of Marine Sediments. Princeton, NJ: Princeton University Press.

Burdige, D. J. 2007. The preservation of organic matter in marine sediments: Controls, mechanisms, and an imbalance in sediment organic carbon budgets? Chem. Rev., *107*(2), 467–485. doi: 10.1021/cr050347q

Burdige, D. J. 2011. The temperature dependence of organic matter remineralization in deeply-buried marine sediments. Earth Planet. Sci. Lett., *311*(3–4), 396–410. doi: 10.1016/j.epsl.2011.09.043

Burdige, D. J., and T. Komada. 2011. Anaerobic oxidation of methane and the stoichiometry of remineralization processes in continental margin sediments. Limnol. Oceanogr., *56*(5), 1781–1796. doi: 10.4319/lo.2011.56.5.1781

Burdige, D. J., and T. Komada. 2015. Sediment pore waters, *in* Biogeochemistry of Marine Dissolved Organic Matter, 2nd ed., D. A. Hansell and C. A. Carlson, eds. Amsterdam: Academic Press, 535–577.

Burdige, D. J., T. Komada, C. Magen, and J. P. Chanton. 2016a. Carbon cycling in Santa Barbara Basin sediments: A modeling study. J. Mar. Res., *74*(3), 133–159. doi: 10.1357/002224016819594818

Burdige, D. J., T. Komada, C. Magen, and J. P. Chanton. 2016b. Modeling studies of dissolved organic matter cycling in Santa Barbara Basin (CA, USA) sediments. Geochim. Cosmochim. Acta, *195*, 100–119. doi: 10.1016/j.gca.2016.09.007

Canfield, D. E., B. Thamdrup, and E. Kristensen. 2005. Aquatic Geomicrobiology. San Diego, CA: Academic Press.

Chanton, J. P., L. C. Chasar, P. Glaser, and D. I. Siegel. 2005. Carbon and hydrogen isotopic effects in microbial methane from terrestrial environments, *in* Stable Isotopes and Biosphere-Atmosphere Interactions, L. B. Flanagan, J. R. Ehleringer, and D. E. Pataki, eds. Amsterdam: Academic Press, 85–105.

Chernyavsky, B. M., and U. G. Wortmann. 2007. REMAP: A reaction transport model for isotope ratio calculations in porous media. Geochem. Geophys. Geosyst., *8*(2), Q02009. doi: 10.1029/2006GC001442

Conrad, R. 2005. Quantification of methanogenic pathways using stable carbon isotopic signatures: a review and a proposal. Org. Geochem., *36*(5), 739–752. doi: 10.1016/j.orggeochem.2004.09.006

Conrad, R., P. Claus, A. Chidthaisong, Y. Lu, A. F. Scavino, Y. Liu, R. Angel, et al. 2014. Stable carbon isotope biogeochemistry of propionate and acetate in methanogenic soils and lake sediments. Org. Geochem., *73*, 1–7. doi: 10.1016/j.orggeochem.2014.03.010

Corbett, J. E., D. J. Burdige, M. M. Tfaily, A. R. Dial, W. T. Cooper, P. H. Glaser, and J. P. Chanton. 2013a. Surface production fuels deep heterotrophic respiration in northern peatlands. Global Biogeochem. Cycles, *27*(4), 1163–1174. doi: 10.1002/2013GB004677

Corbett, J. E., M. M. Tfaily, D. J. Burdige, W. T. Cooper, P. H. Glaser, and J. P. Chanton. 2013b. Partitioning pathways of CO_2 production in peatlands with stable carbon isotopes. Biogeochemistry, *114*(1), 327–340. doi: 10.1007/s10533-012-9813-1

Dale, A. W., P. Regnier, N. J. Knab, B. B. Jørgensen, and P. Van Cappellen. 2008. Anaerobic oxidation of methane (AOM) in marine sediments from the Skagerrak (Denmark): II. Reaction-transport modeling. Geochim. Cosmochim. Acta, *72*(12), 2880–2894. doi: 10.1016/j.gca.2007.11.039

Dickens, G. R. 2011. Down the Rabbit Hole: Toward appropriate discussion of methane release from gas hydrate systems during the Paleocene-Eocene thermal maximum and other past hyperthermal events. Clim. Past, *7*, 831–846. doi:10.5194/cp-7-831-2011

Emery, K. O. 1960. The Sea off Southern California. New York: John Wiley and Sons.

Fenchel, T., G. M. King, and T. H. Blackburn. 1998. Bacterial Biogeochemistry: The Ecophysiology of Mineral Cycling. San Diego, CA: Academic Press.

Gu, G., G. R. Dickens, G. Bhatnagar, F. S. Colwell, G. J. Hirasaki, and W. G. Chapman. 2011. Abundant Early Palaeogene marine gas hydrates despite warm deep-ocean temperatures. Nat. Geosci., *4*, 848–851. doi: 10.1038/ngeo1301

Hamdan, L. J., P. M. Gillevet, J. W. Pohlman, M. Sikaroodi, J. Greinert, and R. B. Coffin. 2011. Diversity and biogeochemical structuring of bacterial communities across the Porangahau ridge accretionary prism, New Zealand. FEMS Microbiol. Ecol., *77*(3), 518–532. doi: 10.1111/j.1574-6941.2011.01133.x

Hamdi, S., W. E. Schiesser, and G. W. Griffiths. 2007. Method of Lines. Scholarpedia, *2*(7), 2859. doi: 10.4249/scholarpedia.2859

Hein, J. R., W. R. Normark, B. R. McIntyre, T. D. Lorenson, and C. L. Powell II. 2006. Methanogenic calcite, ^{13}C-depleted bivalve shells, and gas hydrate from a mud volcano offshore southern California. Geology, *34*(2), 109–112. doi: 10.1130/G22098.1

Henkel, S., J. M. Mogollón, K. Nöthen, C. Franke, K. Bogus, E. Robin, A. Bahr, et al. 2012. Diagenetic barium cycling in Black Sea sediments – a case study for anoxic marine environments. Geochim. Cosmochim. Acta, *88*, 88–105. doi: 10.1016/j.gca.2012.04.021

Heuer, V. B., M. Krüger, M. Elvert, and K.-U. Hinrichs. 2010. Experimental studies on the stable carbon isotope biogeochemistry of acetate in lake sediments. Org. Geochem., *41*(1), 22–30. doi: 10.1016/j.orggeochem.2009.07.004

Hill, T. M., J. P. Kennett, and H. J. Spero. 2004. High-resolution records of methane hydrate dissociation: ODP Site 893, Santa Barbara Basin. Earth Planet. Sci. Lett., *223*(1–2), 127–140. doi: 10.1016/j.epsl.2004.04.003

Hoehler, T. M., M. J. Alperin, D. B. Albert, and C. S. Martens. 1998. Thermodynamic control on hydrogen concentrations in anoxic sediments. Geochim. Cosmochim. Acta, *62*(10), 1745–1756. doi: 10.1016/S0016-7037(98)00106-9

Hoehler, T. M., W. S. Borowski, M. J. Alperin, N. M. Rodriquez, and C. K. Paull. 2000. Model, stable isotope, and radiotracer characterization of anaerobic methane oxidation in gas hydrate-bearing sediments of the Blake Ridge. Proc. Ocean Drill. Program: Sci. Results, *164*, 79–85.

Hornibrook, E. R. C., F. J. Longstaffe, and W. S. Fyfe. 2000. Evolution of stable carbon isotope compositions for methane and carbon dioxide in freshwater wetlands and other anaerobic environments. Geochim. Cosmochim. Acta, *64*(6), 1013–1027. doi: 10.1016/S0016-7037(99)00321-X

Houghton, J. 2015. Global Warming, The Complete Briefing, 5th ed. Cambridge: Cambridge University Press.

Keeling, R. F., A. Körtzinger, and N. Gruber. 2009. Ocean deoxygenation in a warming world. Annu. Rev. Mar. Sci., *2*, 199–229. doi: 10.1146/annurev.marine.010908.163855

Kelley, C. A., J. P. Chanton, and B. M. Bebout. 2015. Rates and pathways of methanogenesis in hypersaline environments as determined by ^{13}C-labeling. Biogeochemistry, *126*(3), 329–341. doi: 10.1007/s10533-015-0161-9

Kelley, C. A., B. E. Nicholson, C. S. Beaudoin, A. M. Detweiler, and B. M. Bebout. 2014. Trimethylamine and organic matter additions reverse substrate limitation effects on the δ^{13}C values of methane produced in hypersaline microbial mats. Appl. Environ. Microbiol., *80*(23), 7316–7323. doi: 10.1128/AEM.02641-14

Kessler, J. D., W. S. Reeburgh, D. L. Valentine, F. S. Kinnaman, E. T. Peltzer, P. G. Brewer, J. Southon, and S. C. Tyler. 2008. A survey of methane isotope abundance (^{14}C, ^{13}C, ^{2}H) from five nearshore marine basins that reveals unusual radiocarbon levels in subsurface waters. J. Geophys. Res.: Oceans, *113*, C12021. doi: 10.1029/2008JC004822

Knab, N. J., B. A. Cragg, E. R. C. Hornibrook, L. Holmkvist, R. D. Pancost, C. Borowski, R. J. Parkes, and B. B. Jørgensen. 2009. Regulation of anaerobic methane oxidation in sediments of the Black Sea. Biogeosciences, *6*(8), 1505–1518. doi: 10.5194/bg-6-1505-2009

Komada, T., D. J. Burdige, S. M. Crispo, E. R. M. Druffel, S. Griffin, L. Johnson, and D. Le. 2013. Dissolved organic carbon dynamics in anaerobic sediments of the Santa Monica Basin. Geochim. Cosmochim. Acta, *110*, 253–273. doi: 10.1016/j.gca.2013.02.017

Komada, T., D. J. Burdige, H.-L. Li, C. Magen, J. P. Chanton, and A. K. Cada. 2016. Organic matter cycling across the sulfate-methane transition zone of the Santa Barbara Basin, California Borderland. Geochim. Cosmochim. Acta, *176*, 259–278. doi: 10.1016/j.gca.2015.12.022

Lapham, L., L. Proctor, and J. Chanton. 1999. Using respiration rates and stable carbon isotopes to monitor the biodegradation of Orimulsion by marine benthic bacteria. Environ. Sci. Technol., *33*(12), 2035–2039. doi: 10.1021/es981158a

Leifer, I., B. P. Luyendyk, J. Boles, and J. F. Clark. 2006. Natural marine seepage blowout: Contribution to atmospheric methane. Global Biogeochem. Cycles, *20*, GB3008. doi: 10.1029/2005GB002668

Lloyd, K. G., M. J. Alperin, and A. Teske. 2011. Environmental evidence for net methane production and oxidation in putative ANaerobic MEthanotrophic (ANME) archaea. Environ. Microbiol., *13*(9), 2548–2564. doi: 10.1111/j.1462-2920.2011.02526.x

Lovley, D. R., and S. Goodwin. 1988. Hydrogen concentrations as an indicator of the predominant terminal electron-accepting reactions in aquatic sediments. Geochim. Cosmochim. Acta, *52*(12), 2993–3003. doi: 10.1016/0016-7037(88)90163-9

Martens, C. S., D. B. Albert, and M. J. Alperin. 1998. Biogeochemical processes controlling methane in gassy coastal sediments—Part 1. A model coupling organic matter flux to gas production, oxidation and transport. Cont. Shelf Res., *18*(14–15), 1741–1770. doi: 10.1016/S0278-4343(98)00056-9

Martens, C. S., D. B. Albert, and M. J. Alperin. 1999. Stable isotope tracing of anaerobic methane oxidation in the gassy sediments of Eckernförde Bay, German Baltic Sea. Am. J. Sci., *299*(7–9), 589–610. doi: 10.2475/ajs.299.7-9.589

Megonigal, J. P., M. E. Hines, and P. T. Visscher. 2003. Anaerobic metabolism: Linkages to trace gases and aerobic processes, *in* Treatise on Geochemistry, H. D. Holland and K. K. Turekian, eds. Oxford: Pergamon, 317–424.

Neubauer, S. C., and J. P. Megonigal. 2015. Moving beyond global warming potentials to quantify the climatic role of ecosystems. Ecosystems, *18*(6), 1000–1013. doi: 10.1007/s10021-015-9879-4

Normark, W. R., D. J. W. Piper, and R. Sliter. 2006. Sea-level and tectonic control of middle to late Pleistocene turbidite systems in Santa Monica Basin, offshore California. Sedimentology, *53*(4), 867–897. doi: 10.1111/j.1365-3091.2006.00797.x

Parkes, R. J., P. Wellsbury, I. D. Mather, S. J. Cobb, B. A. Cragg, E. R. C. Hornibrook, and B. Horsfield. 2007. Temperature activation of organic matter and minerals during burial has been the potential to sustain the deep biosphere over geological timescales. Org. Geochem., *38*(6), 845–852. doi: 10.1016/j.orggeochem.2006.12.011

Paull, C. K., T. D. Lorenson, W. S. Borowski, W. Ussler III, K. Olsen, and N. M. Rodriguez. 2000. 7. Isotopic composition of CH_4, CO_2 species, and sedimentary organic matter within samples from the Blake Ridge: Gas source implications. Proc. Ocean Drill. Program: Sci. Results, *164*, 67–78.

Paull, C. K., W. R. Normark, W. Ussler III, D. W. Caress, and R. Keaten. 2008. Association among active seafloor deformation, mound formation, and gas hydrate growth and accumulation within the seafloor of the Santa Monica Basin, offshore California. Mar. Geol., *250*(3–4), 258–275. doi: 10.1016/j.margeo.2008.01.011

Payne, J. L., D. J. Lehrmann, J. Wei, M. J. Orchard, D. P. Schrag, and A. H. Knoll. 2004. Large perturbations of the carbon cycle during recovery from the end-Permian extinction. Science, *305*(5683), 506–509. doi: 10.1126/science.1097023

Pohlman, J. W., M. Riedel, J. E. Bauer, E. A. Canuel, C. K. Paull, L. Lapham, K. S. Grabowski, R. B. Coffin, and G. D. Spence. 2013. Anaerobic methane oxidation in low-organic content methane seep sediments. Geochim. Cosmochim. Acta, *108*, 184–201. doi: 10.1016/j.gca.2013.01.022

Pohlman, J. W., C. Ruppel, D. R. Hutchinson, R. Downer, and R. B. Coffin. 2008. Assessing sulfate reduction and methane cycling in a high salinity pore water system in the northern Gulf of Mexico. Mar. Pet. Geol., *25*(9), 942–951. doi: 10.1016/j.marpetgeo.2008.01.016

Reeburgh, W. S. 2007. Oceanic methane biogeochemistry. Chem. Rev., *107*(2), 486–513. doi: 10.1021/cr050362v

Rees, C. E. 1973. A steady-state model for sulphur isotope fractionation in bacterial reduction processes. Geochim. Cosmochim. Acta, *37*(5), 1141–1162. doi: 10.1016/0016-7037(73)90052-5

Reimers, C. E., K. C. Ruttenberg, D. E. Canfield, M. B. Christiansen, and J. B. Martin. 1996. Porewater pH and authigenic phases formed in the uppermost sediments of the Santa Barbara Basin. Geochim. Cosmochim. Acta, *60*(21), 4037–4057. doi: 10.1016/S0016-7037(96)00231-1

Schiesser, W. E. 1991. The Numerical Method of Lines: Integration of Partial Differential Equations. San Diego, CA: Academic Press.

Schulz, H. D., and M. Zabel, eds. 2006. Marine Geochemistry, 2nd ed. Berlin: Springer-Verlag.

Shoemaker, J. K., and D. P. Schrag. 2010. Subsurface characterization of methane production and oxidation from a New Hampshire wetland. Geobiology, *8*(3), 234–243. doi: 10.1111/j.1472-4669.2010.00239.x

Sholkovitz, E. 1973. Interstitial water chemistry of the Santa Barbara Basin sediments. Geochim. Cosmochim. Acta, *37*(9), 2043–2073. doi: 10.1016/0016-7037(73)90008-2

Soutar, A., and P. A. Crill. 1977. Sedimentation and climatic patterns in the Santa Barbara Basin during the 19th and 20th centuries. Geol. Soc. Am. Bull., *88*(8), 1161–1172. doi: 10.1130/0016-7606(1977)88<1161:SACPIT>2.0.CO;2

Treude, T., S. Krause, J. Maltby, A. W. Dale, R. Coffin, and L. J. Hamdan. 2014. Sulfate reduction and methane oxidation activity below the sulfate-methane transition zone in Alaskan Beaufort Sea continental margin sediments: Implications for deep sulfur cycling. Geochim. Cosmochim. Acta, *144*, 217–237. doi: 10.1016/j.gca.2014.08.018

Ussler, W., III, and C. K. Paull. 2008. Rates of anaerobic oxidation of methane and authigenic carbonate mineralization in methane-rich deep-sea sediments inferred from models and geochemical profiles. Earth Planet. Sci. Lett., *266*(3–4), 271–287. doi: 10.1016/j.epsl.2007.10.056

Wallmann, K., G. Aloisi, M. Haeckel, A. Obzhirov, G. Pavlova, and P. Tishchenko. 2006. Kinetics of organic matter degradation, microbial methane generation, and gas hydrate formation in anoxic marine sediments. Geochim. Cosmochim. Acta, *70*(15), 3905–3927. doi: 10.1016/j.gca.2006.06.003

Wellsbury, P., K. Goodman, T. Barth, B. A. Cragg, S. P. Barnes, and R. J. Parkes. 1997. Deep marine biosphere fuelled by increasing organic matter availability during burial and heating. Nature, *388*, 573–576.

Whiticar, M. J. 1999. Carbon and hydrogen isotope systematics of bacterial formation and oxidation of methane. Chem. Geol., *161*(1–3), 291–314.

Yoshinaga, M. Y., T. Holler, T. Goldhammer, G. Wegener, J. W. Pohlman, B. Brunner, M. M. M. Kuypers, K.-U. Hinrichs, and M. Elvert. 2014. Carbon isotope equilibration during sulphate-limited anaerobic oxidation of methane. Nat. Geosci., *7*, 190–194. doi: 10.1038/ngeo2069

Zeebe, R. E., and D. Wolf-Gladrow. 2001. CO_2 in Seawater: Equilibrium, Kinetics and Isotopes. Amsterdam: Elsevier.

Received: *16 June 2016*; revised: *23 January 2017*.